NEUTRON-NEUTRON ANGULAR CORRELATION IN ^{252}Cf SPONTANEOUS FISSION

BY

J.S. PRINGLE

A thesis submitted in partial fulfilment
of the requirements for the degree of
Master of Science at the University of
Cape Town

May, 1974

ABSTRACT

The angular correlation between prompt neutrons emitted in ^{252}Cf spontaneous fission has been measured. The observed correlation is compared with a theoretical calculation based on the evaporation model of neutron emission. It is found that the evaporation model is unable to account for the observed strong peaking in the n-n angular correlation at small angles.

Preliminary calculations show that two of the proposed alternative neutron emission mechanisms, polar emission and "tidal wave" emission, may be able to account for the observed n-n angular correlation.

ACKNOWLEDGEMENTS

I wish to express my appreciation and gratitude to:

Professor F.D. Brooks, my supervisor, for both his help and guidance during the project and his advice on the compilation of this thesis;

Professor I.J. van Heerden, Head of the Southern Universities Nuclear Institute, for the use of the Institute's facilities;

Miss P. Partridge, for typing the manuscript and preparing the diagrams;

My parents, for their support and encouragement.

------oOo------

TABLE OF CONTENTS

CHAPTER ONE

INTRODUCTION

1.1 Motivation for the Present Work

Since the discovery by Hahn and Strassmann (Ha 39) of nuclear fission in 1938, a massive effort has been made towards gaining a better understanding of the fission process. The study of fission is of fundamental importance in nuclear physics since it yields knowledge of the nuclear structure of highly deformed nuclei. As yet there is no completely satisfactory theory of nuclear fission. The Liquid Drop Model (LDM) developed by Bohr and Wheeler (Bo 39) successfully explains qualitatively most of the observed features of fission but fails to explain the striking asymmetry of the fission fragment mass distribution. There is recent evidence to show that this failure arises as a result of neglecting the internal structure of the nucleus (Ra 71).

In the LDM the short-range, charge independent, forces between the individual nucleons of the nucleus are represented by the surface tension of the drop. An undeformed nucleus assumes a spherical shape which is the result of a balance between the repulsive Coulomb forces between the protons and the attractive nucleon-nucleon forces represented by the surface tension. This balance sets up a fission barrier which may be crossed if sufficient excitation energy is added to the nucleus (drop) so that the repulsive Coulomb forces exceed the attractive surface tension. The necessary excitation energy may be provided by adding a neutron to the nucleus (neutron-induced fission). Alternatively, in analogy with alpha decay, the fission process may proceed via barrier penetration (spontaneous fission).

Fissions by means of these two processes have similar characteristics. Bearing this in mind, information drawn from studies of neutron-induced fission has been included in the following discussion, even though the project described in this thesis concerns only spontaneous fission.

When the fission barrier is penetrated, the nucleus breaks up in about

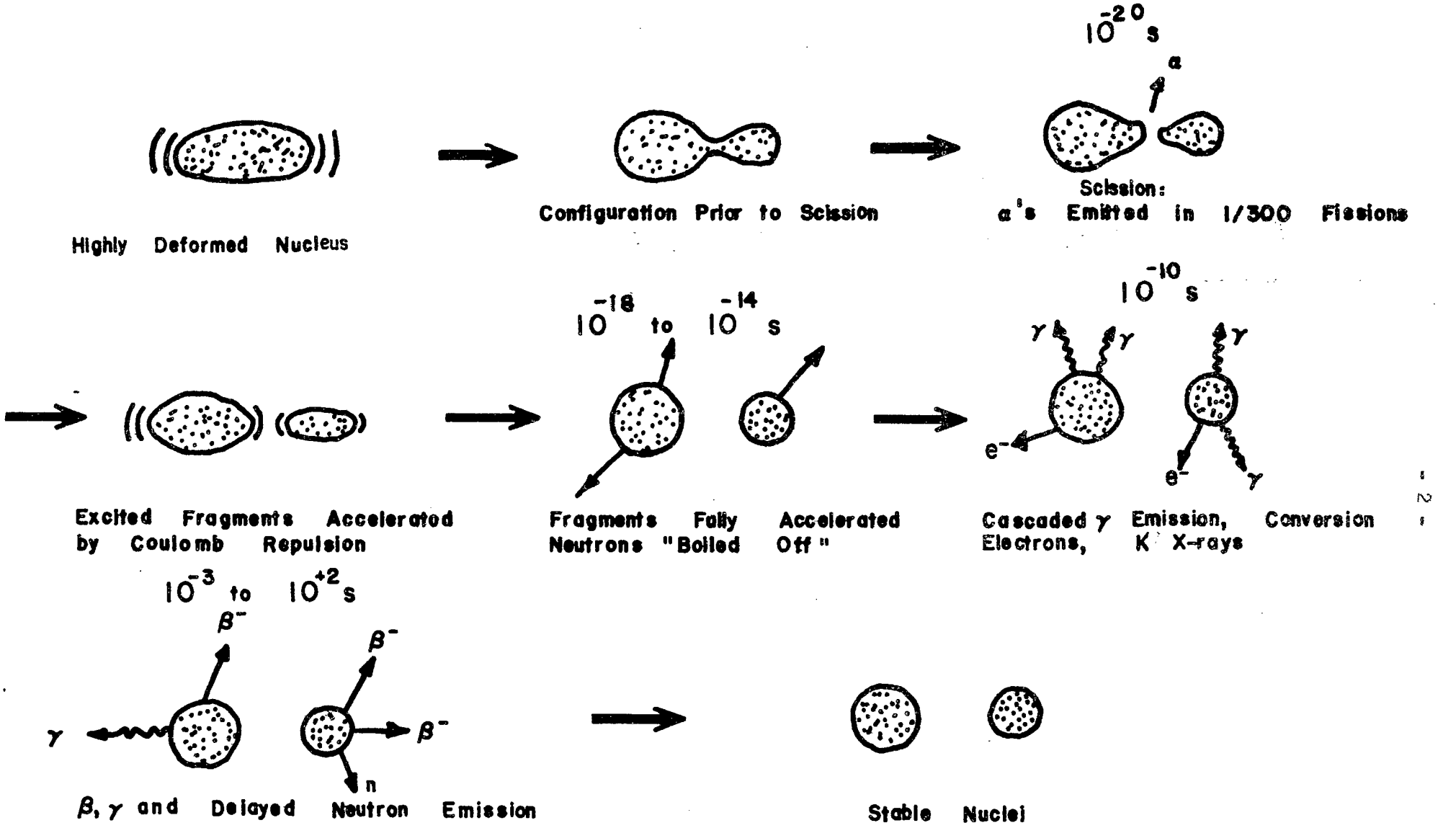

Fig. 1.1: Schematic Diagram of Fission

10^{-20} seconds. Binary fission, resulting in the formation of two highly excited fission fragments, is overwhelmingly predominant as the fission mode. The two fragments created by the nuclear breakup are forced apart by the repulsive Coulomb force between them. In rare cases, a charged particle may be emitted at the instant of scission (i.e. when the neck joining the two "fragments" snaps). The extra particle produced in this ternary fission mode is nearly always an alpha. The relative abundance of ternary to binary fission modes in the case of ^{252}Cf spontaneous fission is about 1 in 300 (No 62).

As the fission fragments assume a stable spherical shape their deformation energy is converted into excitation energy. The fragments then de-excite by "boiling off" neutrons in about 10^{-18} to 10^{-14} seconds and a cascade emission of gamma rays in about 10^{-10} seconds after scission. A small percentage of the gamma transitions are internally converted in the K shell leading to the emission of conversion electrons and K X-rays. In the time interval 10^{-3} to 10^{+2} seconds after scission the neutron rich fragments undergo beta decays and emit delayed neutrons and gamma rays, finally ending up as stable nuclei. The fission process is shown schematically in fig. 1.1.

It is clear that the study of the radiations emitted at different stages of the fission process can yield much information about the fundamental nature of fission. This thesis sets out to investigate an aspect of prompt neutron emission from individual fragments in ^{252}Cf spontaneous fission.

Several research groups (e.g., Mi 58, Bo 62, Sc 65) have made detailed studies of ^{252}Cf spontaneous fission, revealing two dominant features (which are characteristic for low energy fission of all fissioning nuclei with mass number between 230 and 254). These are: (1) the enormous preference for the nucleus to break up into two fragments of unequal mass; and, (2) the sharp discontinuity in the prompt neutron yield curve in the region of symmetric

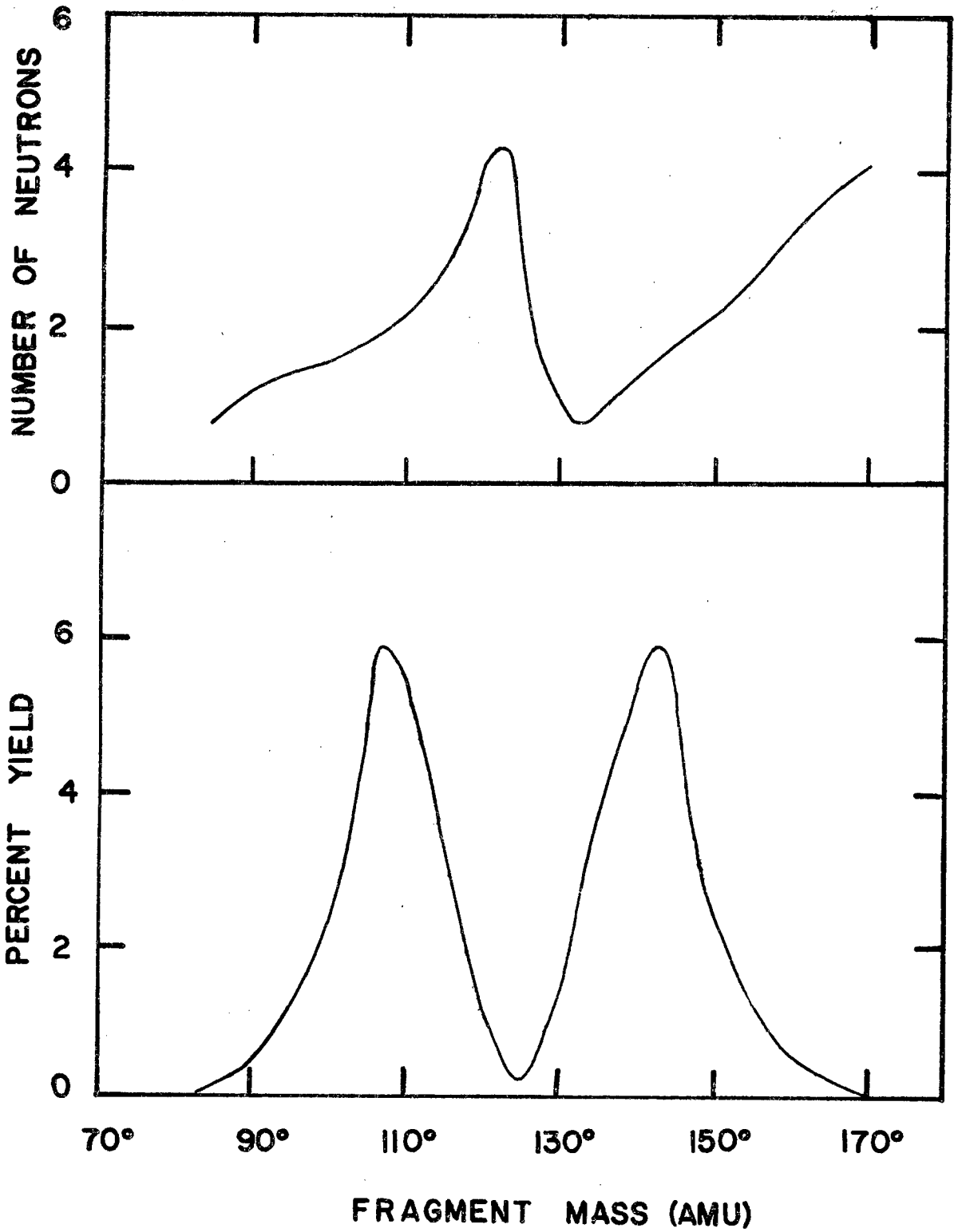

Fig. 1.2: The Two Dominant Features of Low Energy Fission sketched here for ^{252}Cf Spontaneous Fission.
above: the Saw-Tooth Neutron Yield Curve
below: the Double Humped Mass Distribution

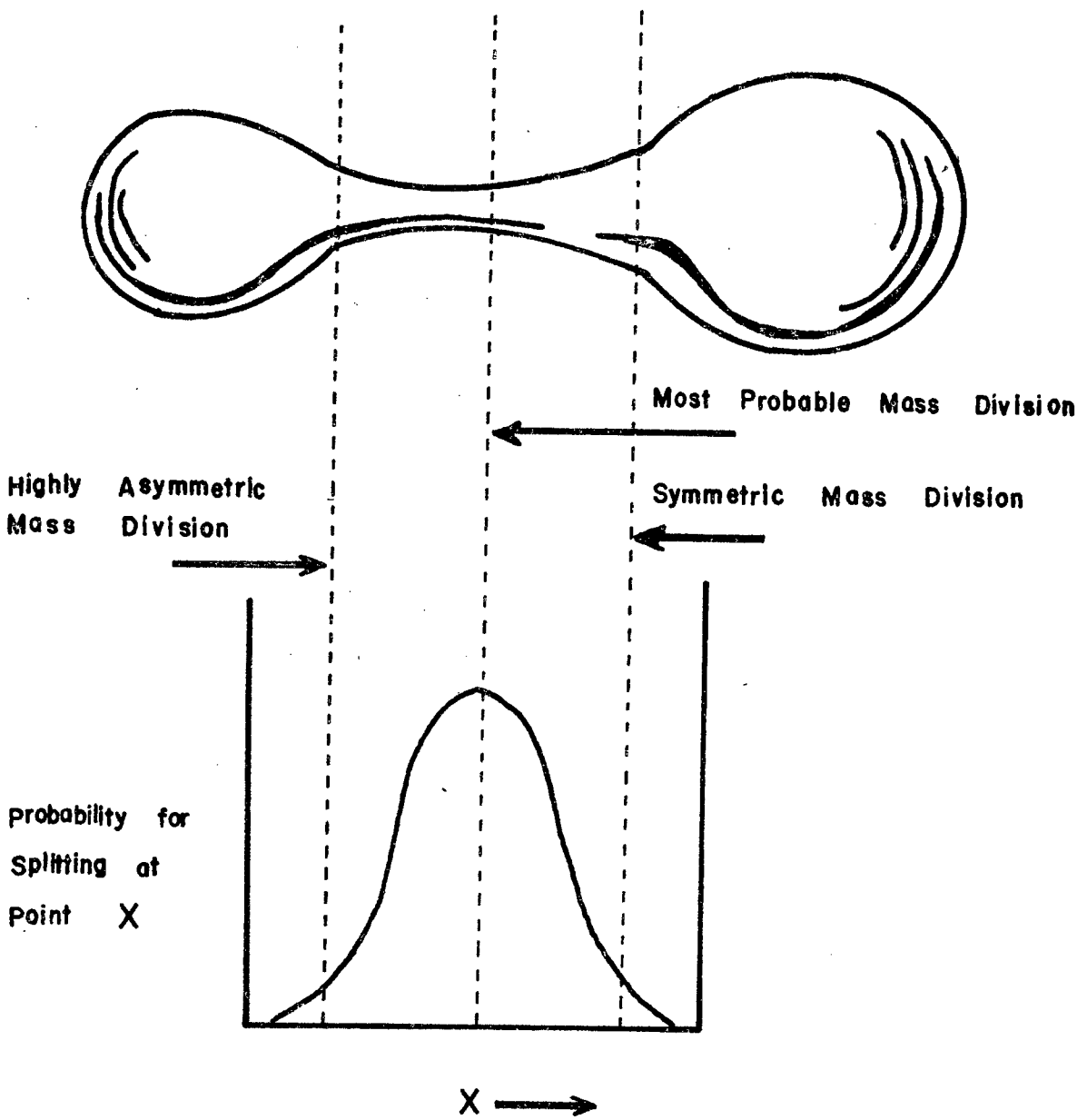

Fig. 1.3: Whetstone's Model of the Fissioning Nucleus Shortly Before Scission

fission, resulting in a saw-tooth neutron yield vs. fragment mass distribution. These two distributions are sketched in fig. 1.2.

It is seen that for ^{252}Cf spontaneous fission the predominant asymmetric mode of mass division leads, on average, to the emission of 2 neutrons from each fragment. Near-symmetric division is rare and will result in the emission of about 4 neutrons from the light fragment and none from the heavy fragment. Whetstone (Wh 59) has devised a model, illustrated in fig. 1.3, to explain this observation.

In the Whetstone model the fissioning nucleus is pictured, immediately prior to scission, as being made up of two lumps of nuclear matter, more often than not of unequal volume, joined by a fairly long neck. This neck contains the number of nucleons equal to the difference in mass between the mean light and heavy fragments. The most likely place for the neck to snap is in the middle, and when this occurs two asymmetric masses having nearly equal excitation energies are formed. Since the deformed nucleus is virtually "cold" at the scission point this means that these fragments emit comparable numbers of neutrons. In rare cases the neck snaps very close to the large lobe, resulting in a near-symmetric mass division. When this happens the light fragment carries off virtually all of the deformation energy and as a result emits many more neutrons than the heavy fragment. This model thus explains the double peaked fragment mass distribution and the saw-tooth neutron yield curve.

The angular distribution of fission neutrons relative to the fragment axis; i.e. the axis defined by the fragment directions, was first measured for ^{235}U fission by Wilson (Wi 47) in 1945. The dominant feature of this distribution is a strong peaking in the directions of motion of the two fragments. Later measurements by Fraser (Fr 52) on thermal neutron-induced fission of ^{233}U, ^{235}U and ^{239}Pu, Kapoor et al (Ka 63) and Skarsvåg and

Bergheim (Sk 63) on ^{235}U, and Bowman et al (Bo 62) on spontaneous fission of ^{252}Cf have all confirmed this feature. The results are broadly consistent with the isotropic evaporation of the neutrons in the fully accelerated frames of their parent fragments. However there are deviations from this picture.

Bowman et al (Bo 62) found that in ^{252}Cf spontaneous fission the number of neutrons emitted at 11.25°, 90° and 168.75° to the fragment axis was in excess of that expected from the evaporation model. It was found on analysis of the data that there was no marked anisotropy in the emission of neutrons from the fragments. The excess of neutrons at 90° to the fragment axis was explained by assuming that a small fraction (about 10%) of the neutrons are not emitted from the fragments but from the fissioning nucleus. These neutrons were termed scission neutrons and were first suggested by Bohr and Wheeler (Bo 39). With the exception of the data at 11.25° and 168.75°, good agreement between the observed and calculated distributions was obtained by assuming that the scission neutrons were emitted isotropically in the laboratory frame, with a Maxwellian energy spectrum having an average energy of about 2.6 Mev. This is slightly higher than the average energy of about 2.2 Mev of the evaporation neutrons in the laboratory frame.

The inclusion of a scission component did not explain the excess of neutrons at small angles to the fragment axis in Bowman's data. It seems unlikely that the excess of neutrons is entirely the result of a systematic experimental error, and Bowman et al (Bo 62) concluded that further experiments were needed to confirm or disprove the existence of a small number of neutrons collimated along the fragment axis.

Skarsvåg and Bergheim (Sk 63) studied the neutron-induced fission of ^{235}U and concluded that about 15% of the fission neutrons are emitted isotropically in the laboratory frame. The energy spectrum of these scission

neutrons was tentatively described by an evaporation spectrum with an average energy of 1.8 Mev. Their data did not indicate any anisotropy in the emission of neutrons from the fragments.

Kapoor et al (Ka 63) concluded from a similar study of ^{235}U fission that about 10% of the emitted neutrons were scission neutrons having an average energy of 3.2 Mev. Milton and Fraser (Mi 65) estimated that the percentage of scission neutrons in the thermal fission of ^{233}U and ^{235}U may be as high as 30%.

There has been very little new evidence on scission neutrons since these early results were obtained. The available estimates of the percentage of scission neutrons are accompanied by large uncertainties because of the difficulty of distinguishing them from the more copious evaporated neutrons.

Fuller (Fu 62) has shown that neutrons may be emitted in the region between the fragments at the time of scission in the same way that light charged particles are assumed to be emitted in ternary fission. His calculation, in which the nucleus was considered to be a square-well containing a Fermi sea of nucleons, indicated that a nonadiabatic distortion of the potential binding the nucleons in the well would result in an ejection of some neutrons from the well prior to scission. For a set of parameters which were consistent with experimental observations, and a scission time of about 5×10^{-22} seconds, it was found that for the ^{252}Cf nucleus as many as 1.5 neutrons per fission may be emitted by this mechanism.

An alternative mechanism to account for scission neutron emission has been suggested by Nadkarni (Na 71) who speculates that scission neutrons may be evaporated from the distorted nucleus prior to scission during the descent from saddle to scission points.

Whether scission neutrons exist or not, it is generally concluded that

the gross features of neutron emission in low energy fission are well explained in terms of an evaporation model. In the case of ^{252}Cf spontaneous fission at least 90% (if not all) of the fission neutrons appear to be evaporated isotropically from the fully accelerated fragments (Bo 62).

1.1 Motivation for the Present Work

From the evaporation model and the detailed quantitative data upon which this model rests we can predict the angular correlation between fission neutrons, i.e. the probability of observing two neutrons from the same fission, at a given relative angle to one another. A measurement of this correlation should therefore provide a useful test of the model. It would be particularly useful to measure the n-n angular correlation for known values of the angle between the fission axis and one or both neutrons. However even an (experimentally simpler) measurement of this correlation for events in which the fission axis is known to be randomly orientated in space would be useful.

From the evaporation model we would expect neutrons to be emitted randomly in time (over about 10^{-16}s.) and in space in the reference frames of their parent fragments. Therefore by considering fissions one-by-one from a set whose average properties (mass ratio, number of neutrons emitted from each fragment, etc.) conform with those observed for ^{252}Cf spontaneous fission, we can determine the neutron distribution from each fragment (in the fragment frame) in each fission. This distribution can then be transformed to the laboratory frame, in which the fission axis is randomly orientated, by superimposing the individual fragment motions. The neutron-neutron correlation can then be determined from the distribution observed for the full set of fissions.

An extensive literature survey has revealed only one previous experimental

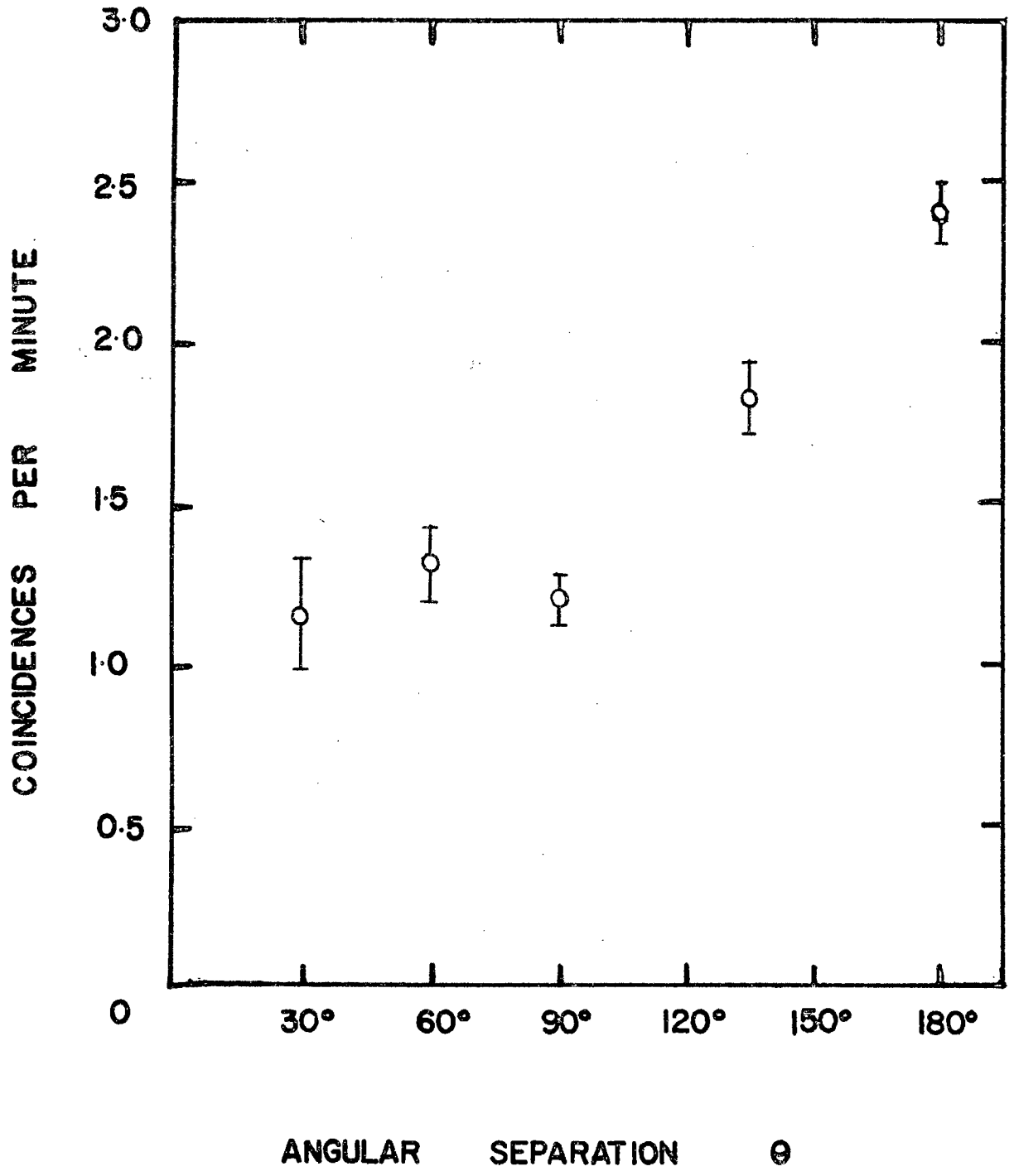

Fig. 1.4: The (Corrected) Measurements of De Benedetti et al (De 48) of the angular distribution of n-n coincidences from the neutron-induced fission of ^{235}U.

investigation of the neutron-neutron angular correlation in fission. In this work, which was carried out in 1948, De Benedetti et al (De 48) measured the angular distribution of neutron-neutron coincidences resulting from the neutron-induced fission of ^{235}U. The experiment was performed using two proportional counters and the fissile sample was a small metal disc which was placed in a "thermal" beam from a nuclear reactor. The coincidence rate was observed for different angular separations of the two counters. After correcting their data for random and false coincidences, De Benedetti et al concluded from their results (fig. 1.4) that for ^{235}U there are at least twice as many neutron pairs emitted by opposite fragments than neutron pairs emitted by the same fragment. However their measurements, being restricted to the five angles, 30°, 60°, 90°, 135° and 180°, would not have been capable of resolving detailed structure in the angular correlation, if such were present. In particular, since these measurements did not extend to angles of less than 30°, any strong correlation in the directions of emission of neutrons from the fragments could not have been detected.

Surprisingly, there appears to have been no follow-up to the work of De Benedetti et al. No further measurements have been reported of neutron-neutron angular correlations in the fission of ^{235}U or any other nucleide.

In terms of the conventional picture of fission as a cataclysmic breakup of the nucleus giving rise to two very highly excited fragments, it is hard to imagine how a directional correlation between the emitted neutrons can arise. However, consistent and unexplained small deviations do exist between the expected and observed neutron angular distribution (e.g. Bowman's (Bo 62) finding of an excess of neutrons at small angles to the fission axis). Without anticipating the results of the present investigation in any way it is relevant at this point to speculate briefly as to how a neutron-neutron

correlation different to that predicted by the evaporation model might occur. Clearly, one must consider whether the possibility of such correlation is not already ruled out by the observed angular distribution of neutrons with respect to the fission axis. Three possible mechanisms which might be considered are the following:

(i) Bunched Emission

In the case of ^{252}Cf spontaneous fission more than 90% of the fissions result in two or more neutrons being emitted from one fragment (Hy 64). It is conceivable that some of these fissions could lead to paired or even bunched emission with two or more neutrons in a state of low relative momentum. If so, then the n-n angular correlation would be enhanced at small angles. Moreover, if the direction of emission of the bunch is random in the fragment frame then the angular distribution of neutrons in this frame, averaged over many fissions, will still be isotropic. Thus the experimental finding (e.g. Bo 62) that the neutron angular distribution is nearly isotropic in the parent fragment frame would not be inconsistent with the neutron-neutron angular correlation resulting from bunched emission.

(ii) Localized Emission of Neutrons

From studies of ternary fission there is evidence (Ha 71) that about 5% of the alpha particles resulting from this fission mode are emitted from the remote poles of the fission fragments, i.e. the poles defined by the fission axis on the far sides of each fragment. The most likely explanation of

the origin of these polar alphas is that they arise from the snapping back of the outer ends of the deformed fragments just after scission. It is conceivable that a similar mechanism could lead to the emission of "collimated" polar neutrons, thereby affecting the neutron-neutron correlation. While it seems more likely that neutron emission by this mechanism will occur near the poles, it is possible that localized emission may occur from any part of the surface of the excited fragment through tidal interference effects.

(iii) Cascaded Emission of Neutrons

It is conceivable that the decay of an excited nucleus by a series of neutron emissions, in analogy to the more familiar case of a gamma-cascade, might lead to a neutron-neutron angular correlation. However it seems highly unlikely that such a process should be important in the decay of fission fragments owing to the variety of fragment configurations produced and the variety of initial states populated in each fragment. Since the experiment necessarily averages over all fragment masses and initial states one would expect that any correlation arising from this source would be averaged out completely.

It would seem therefore that there is some interest in testing the predictions of the evaporation model in regard to the angular correlation of the prompt neutrons from fission. This project aimed to carry out such a test in three stages, firstly by observing the correlation experimentally, secondly by simulating the experiment by means of a Monte Carlo calculation based on

the evaporation model and thirdly by comparing the experimental observations with the results of the calculation.

CHAPTER TWO

EXPERIMENTAL METHODS

2.1 Outline of the Method

The n-n angular correlation for neutrons from ^{252}Cf spontaneous fission was measured using a ^{252}Cf source and a pair of neutron detectors. One detector and the source were kept fixed in the horizontal plane and the other detector was rotated about a vertical axis through the source in order to vary the correlation angle θ (see fig. 2.1). The coincidence rate between the two detectors and their individual singles rates were then determined as a function of θ. The time spectrum of the coincidences was also measured for each run to provide a monitor of the random coincidence background as well as a check on the scaler measurement of the number of coincidences.

For detector-source distances $d_1 = d_2 = 10$ cm this detector configuration (fig. 2.1) gave a range of possible θ's from $\theta_{min} = 20^\circ$ to $\theta_{max} = 260^\circ$. Since it is at small angles that any n-n correlation effects (if they exist) are expected to be seen, measurements were also made at angles in the range $\theta = 10^\circ$ to $\theta = 20^\circ$ by increasing d_1 and d_2 to 18 cm. ($\theta_{min} = 10^\circ$ at 18 cm.)

2.2 The Sources

Californium-252 decays predominantly by alpha emission and only about 3.1% of all decays are by spontaneous fission. The effective half-life considering both modes of decay is 2.65 years (Am 72). On average, each spontaneous fission results in the emission of 3.743 ± 0.016 neutrons (Ha 69).

The ^{252}Cf source used in this experiment was obtained from the Oak Ridge National Laboratory. It is sealed in a stainless steel cylinder (1.6 cm long x 0.3 cm diam.) which is mounted inside an aluminium cylinder (3.9 cm long x 1.3 cm diam.). During the experiment the source was wrapped in a thin (1.6 mm) lead shield to attenuate the gamma radiation. The neutron emission rate from the source was about 6×10^3 neutrons/s when the experiment was performed.

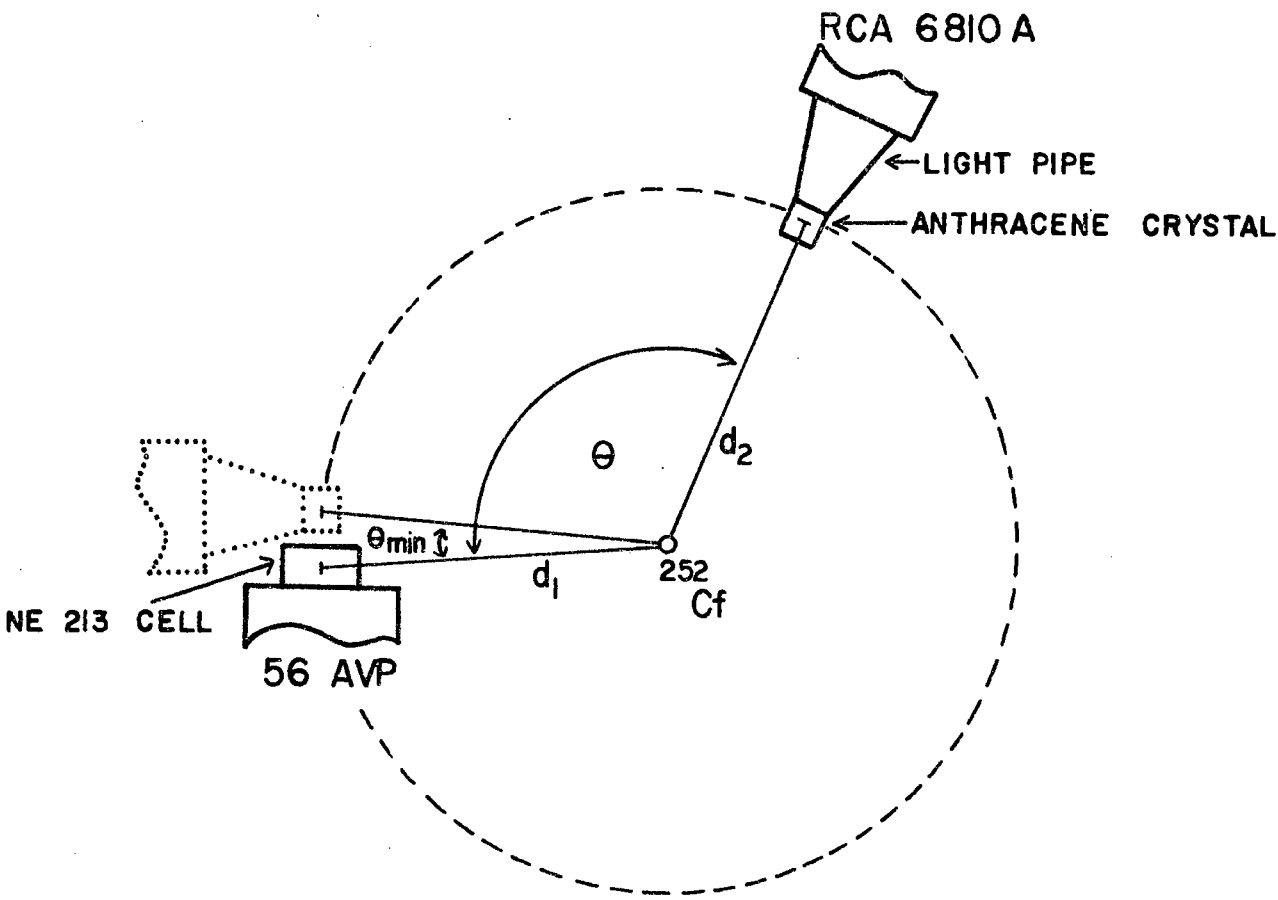

Fig. 2.1: The Detector-Source Geometry

A source of single neutrons was required in order to determine the probability of single neutrons being detected in both detectors after multiple scattering. An Am-Be source which emits neutrons through the nuclear reaction

$$^{9}Be + \alpha \rightarrow ^{12}C + n + 5.71 \text{ Mev}$$

was used for this purpose. The source used emits about 10^6 neutrons/s and is sealed in a stainless steel container 3.0 cm long and 2.1 cm in diameter. This container was also surrounded by a lead shield to attenuate the source gamma radiation.

2.3 The Neutron Detectors

The neutron detectors were organic scintillators. Pulse shape discrimination (PSD) was used to select n-p recoils within the scintillators while rejecting Compton electrons from the gamma ray background. The detectors used were an anthracene crystal ($C_{14}H_{10}$), and the liquid scintillator NE 213 which consists mainly of xylene (C_8H_{10}). Both of these scintillators are known for their excellent PSD properties (e.g. Br 59).

The NE 213 liquid was encapsulated in a cylindrical glass cell 3.8 cm in diameter and 2.5 cm thick, while the anthracene was in the form of a cylindrical crystal 2.5 cm in diameter and 2.5 cm thick.

The two scintillators were mounted on 5 cm diameter photomultiplier tubes. The NE 213 cell was optically coupled to a Phillips 56AVP tube which was kept fixed throughout the experiment. A lucite light pipe was used to couple the anthracene crystal to an RCA 6810A tube. Since this tube was moved during the experiment it was shielded from the Earth's magnetic field by enclosure inside a cylindrical mu-metal shield.

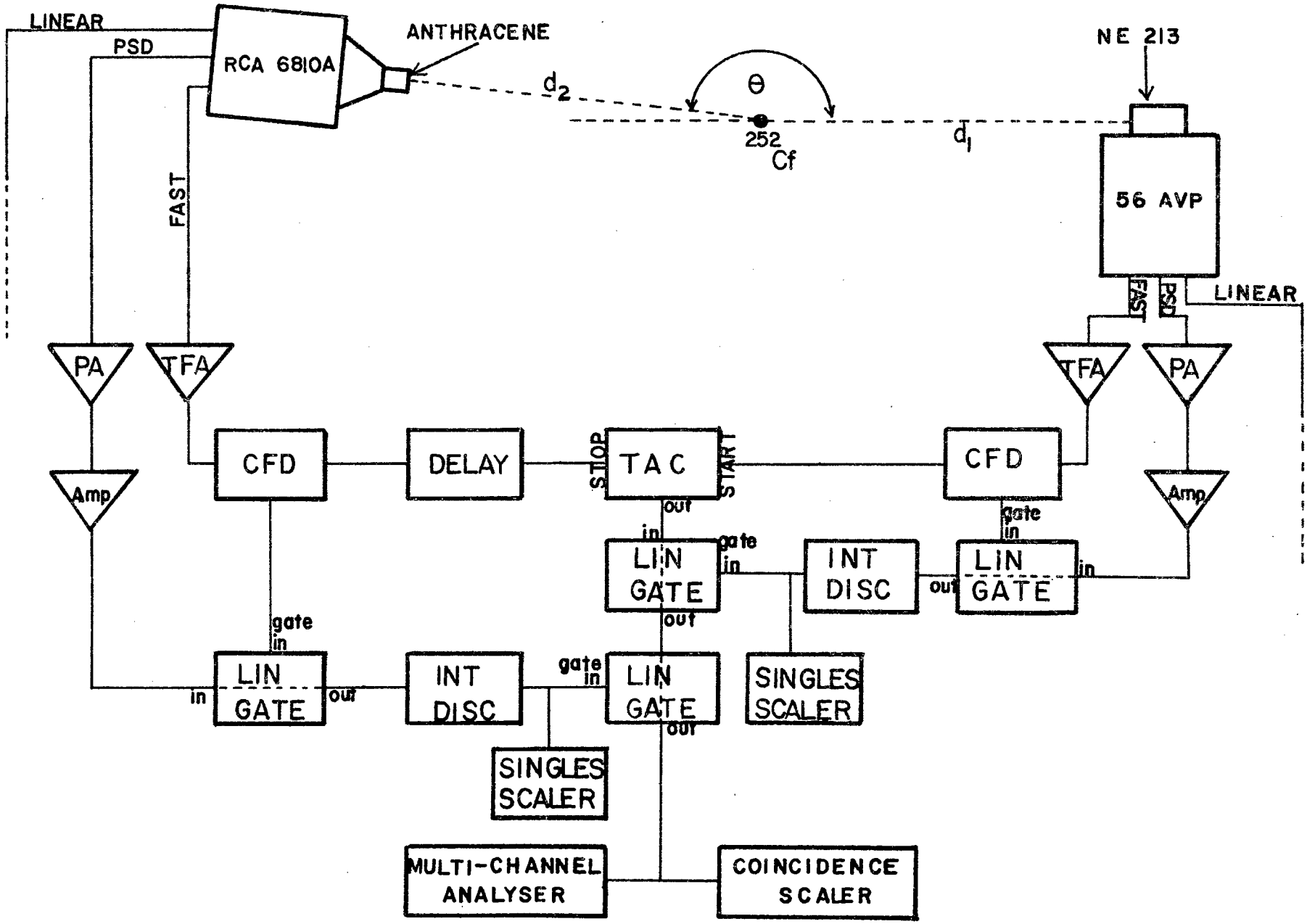

Fig. 2.2: Block Diagram of the Electronic System

2.4 The Electronic System

A block diagram of the electronic system used is shown in fig. 2.2. The PSD systems of the two detectors were adjusted independently using gamma and neutron sources. Then the outputs of both PS discriminators were used to gate the output of the time-to-amplitude converter (TAC) which was thereafter fed to the multichannel analyser (NS 601 or NS 625/630). The two PSD outputs were also scaled, to obtain the two singles rates N_1 and N_2. The coincidence rate N_{co} was recorded by scaling the gated TAC output.

2.5 Gamma Discrimination Efficiency

The efficiency of the PSD system in discriminating against gamma-gamma coincidences was determined using both ^{22}Na and ^{60}Co gamma sources. For each source two coincidence-time spectra were obtained, one with the PSD gating on and one with the PSD off. The results are shown below.

SOURCE	COINCIDENCES IN 200 SECONDS		GAMMA BREAKTHROUGH
	PSD ON	PSD OFF	
^{22}Na	7	38456	0.028%
^{60}Co	2	41574	0.015%

Thus the efficiency of the PSD system for rejecting gamma-gamma coincidences was better than 99.9%.

2.6 Determination of the Operating Bias

It is necessary to know the bias levels of the detectors to calculate their absolute efficiencies. To determine these levels the pulse height scale was calibrated in terms of electron energy using a ^{137}Cs gamma source.

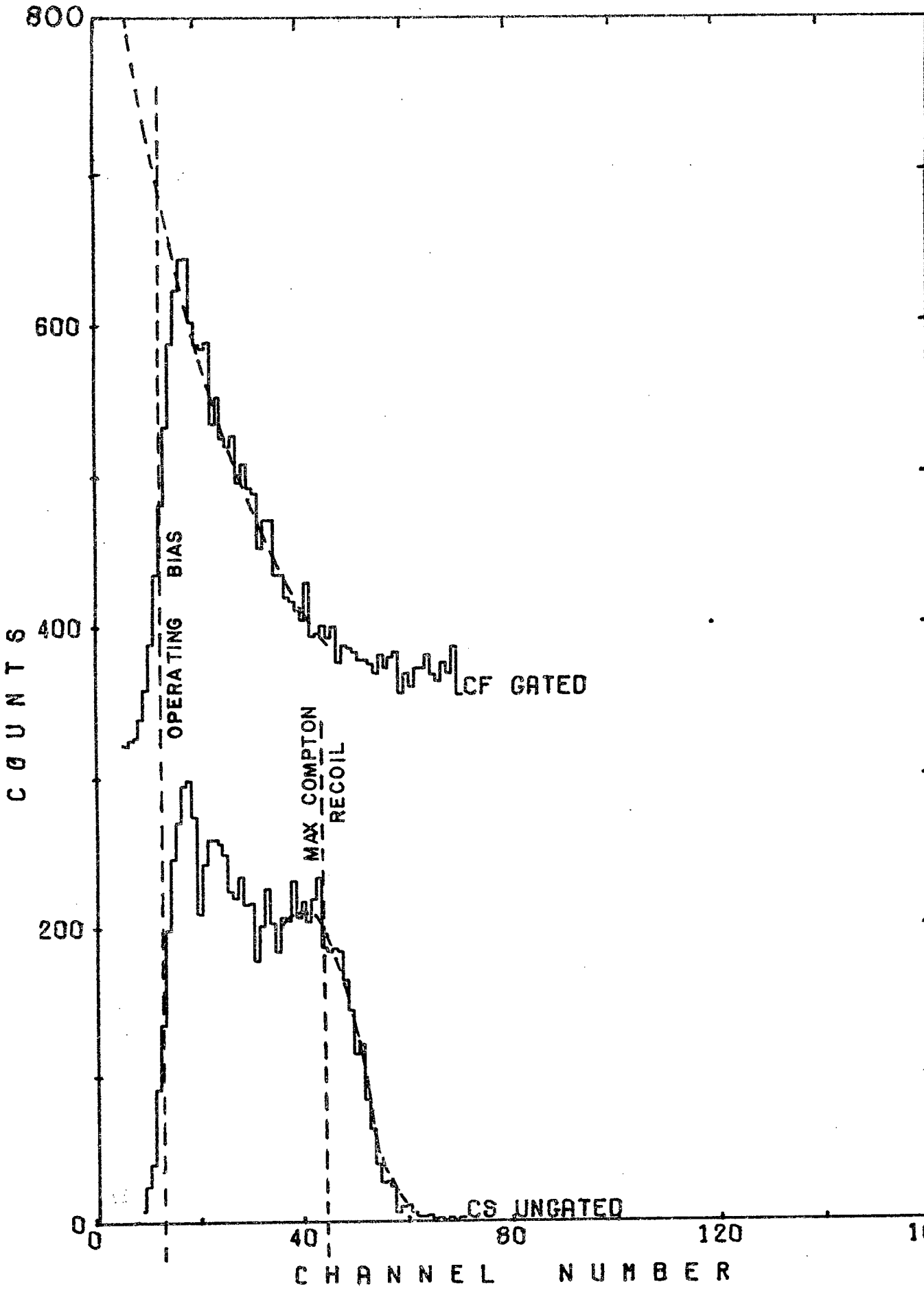

Fig. 2.3: BIAS DETERMINATION FOR ANTHRACENE CRYSTAL

True Zero at Channel Number 3

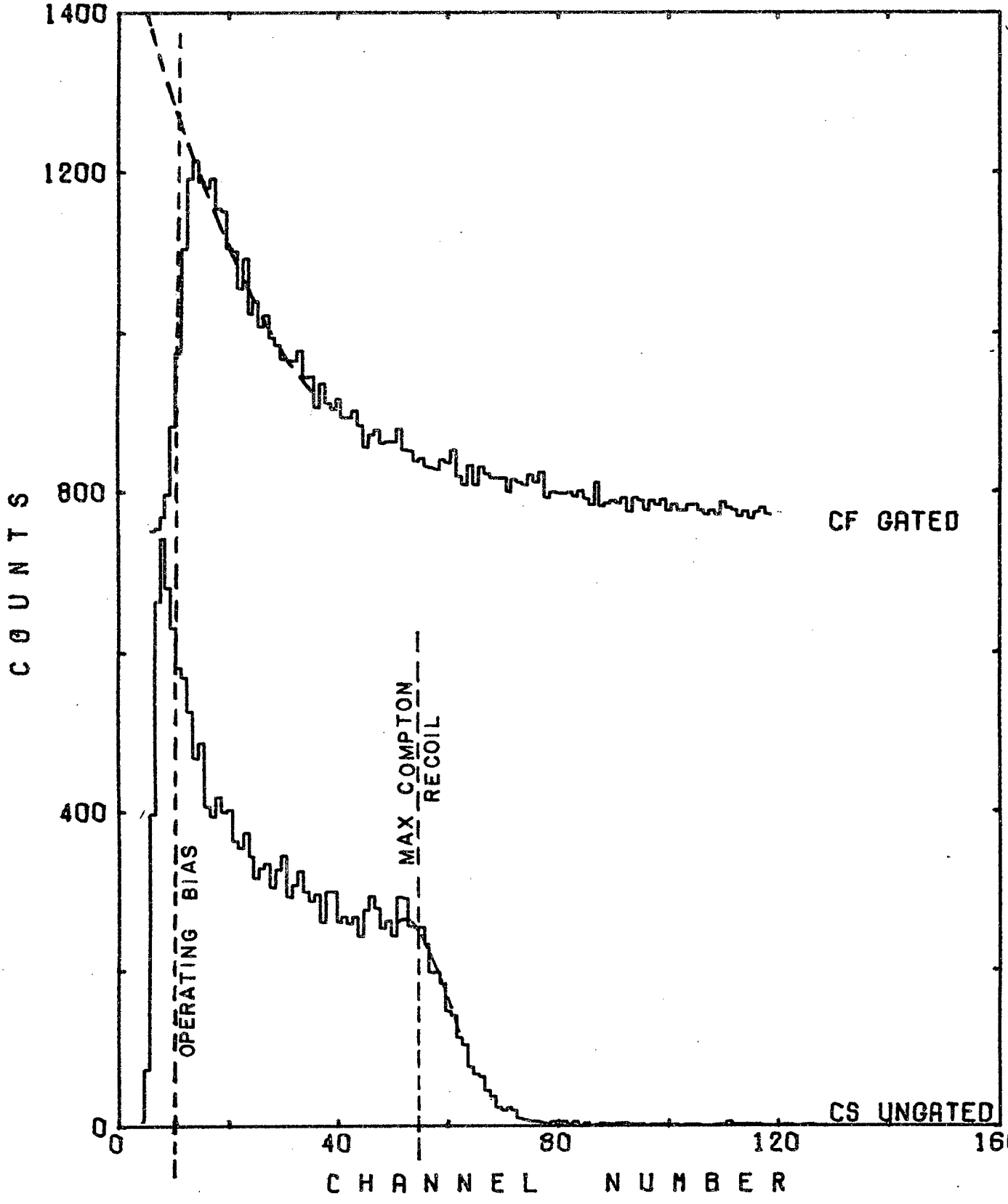

Fig. 2.4: BIAS DETERMINATION FOR NE 213 LIQUID

True Zero at Channel Number 3

The ungated ^{137}Cs and the PSD gated ^{252}Cf spectra for the two detectors are shown in figs. 2.3 and 2.4.

Knox and Miller (Kn 72) have shown that for a 5 cm diameter by 5 cm thick NE 213 scintillator the maximum recoil Compton electron occurs at nearly 90% of the peak of the pulse height distribution. This result has been applied here to the anthracene crystal as well as the NE 213 liquid.

The operating bias was defined as being the proton energy at which the discriminators (PSD or "fast") reduced the recoil proton count from ^{252}Cf neutrons by half. This bias was determined for each detector as shown in figs. 2.3 and 2.4. In the case of the anthracene crystal the operating bias was the fast bias of the detector, while for the NE 213 liquid it was the PSD bias. The maximum energy of the Compton recoil electron for the 0.662 Mev gamma ray of ^{137}Cs is 0.478 Mev. Using this reference point the equivalent electron energies of the operating biases were determined for the two detectors. These in turn were converted to equivalent recoil proton energies and hence neutron energies using the response curves of Brooks (Br 56).

The biases were found to be 0.33 Mev for the NE 213 detector and 0.47 Mev for the anthracene crystal.

2.7 Time Resolution of the System

The time resolution of the apparatus was determined using a ^{22}Na source which emits pairs of annihilation quanta at 180° to each other. In the measurement the detectors were placed face to face with the source between them. Two coincidence-time spectra (shown in fig. 2.5) were measured for the source; one with no delay, and the other with a 20 ns delay introduced into the stop pulse to the TAC. This gave a time calibration of the channel widths.

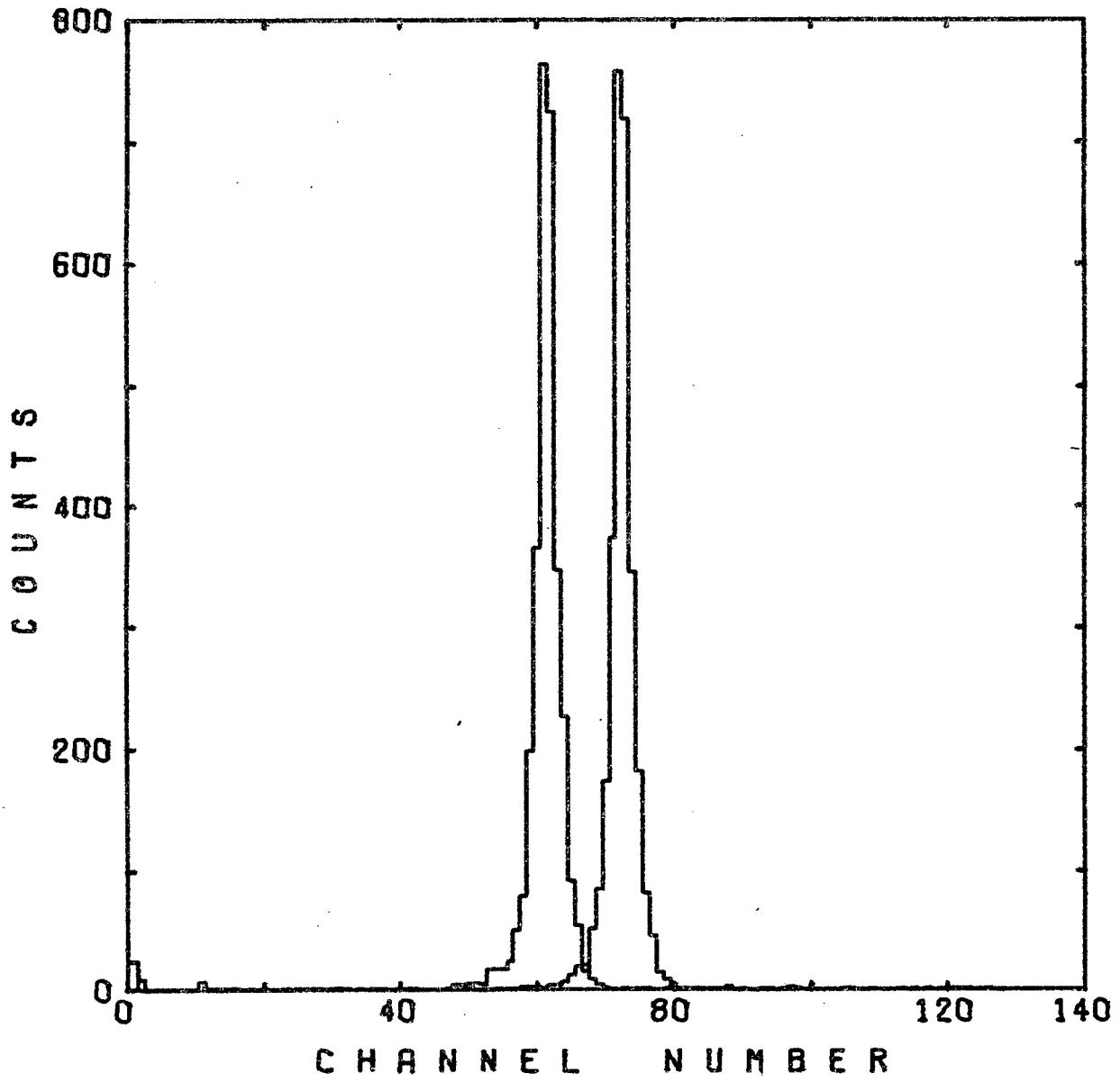

Fig. 2.5: ^{22}Na Coincidence-Time Spectra with 20 ns delay between peaks.

The time resolution, defined as the full width at half the maximum height of the coincidence-time spectrum, was found to be about 5.5 ns. The effective time resolution of the scaler measurements (corresponding to the full range of the time spectrum shown in fig. 2.5) was 230 ns.

2.8 Calculation of Efficiency of Detectors

It is necessary to know the efficiency $\varepsilon(E)$ of the detectors for neutron detection, as a function of neutron energy, for a direct comparison of the experimental results and the computer simulation of the experiment. This was calculated using the formula (Ow 60):

$$\varepsilon(E) = \frac{E - E_B}{E} \left[1 - \exp\left(-n_H \sigma_H(E) x\right) \right]$$

where E = incident neutron energy,

E_B = bias of detector,

n_H = no. of hydrogen atoms /cm^3 in scintillator,

$\sigma_H(E)$ = n-p scattering cross section at neutron energy E,

x = mean thickness of scintillator

This formula takes no account of the effects of multiple n-p scatterings in the scintillator. It also ignores the effects of neutron scatterings off carbon nuclei. These are reasonable assumptions since the light output from recoiling carbon nuclei is extremely small and multiple scattering effects are small in scintillators of the dimensions used.

In the evaluation of the detector efficiencies the following data were used:

DETECTOR	E_B (Mev)	n_H (atoms/cc)	x (cm)
Anthracene	0.47	4.22×10^{22}	2.5
NE 213	0.33	4.60×10^{22}	3.0

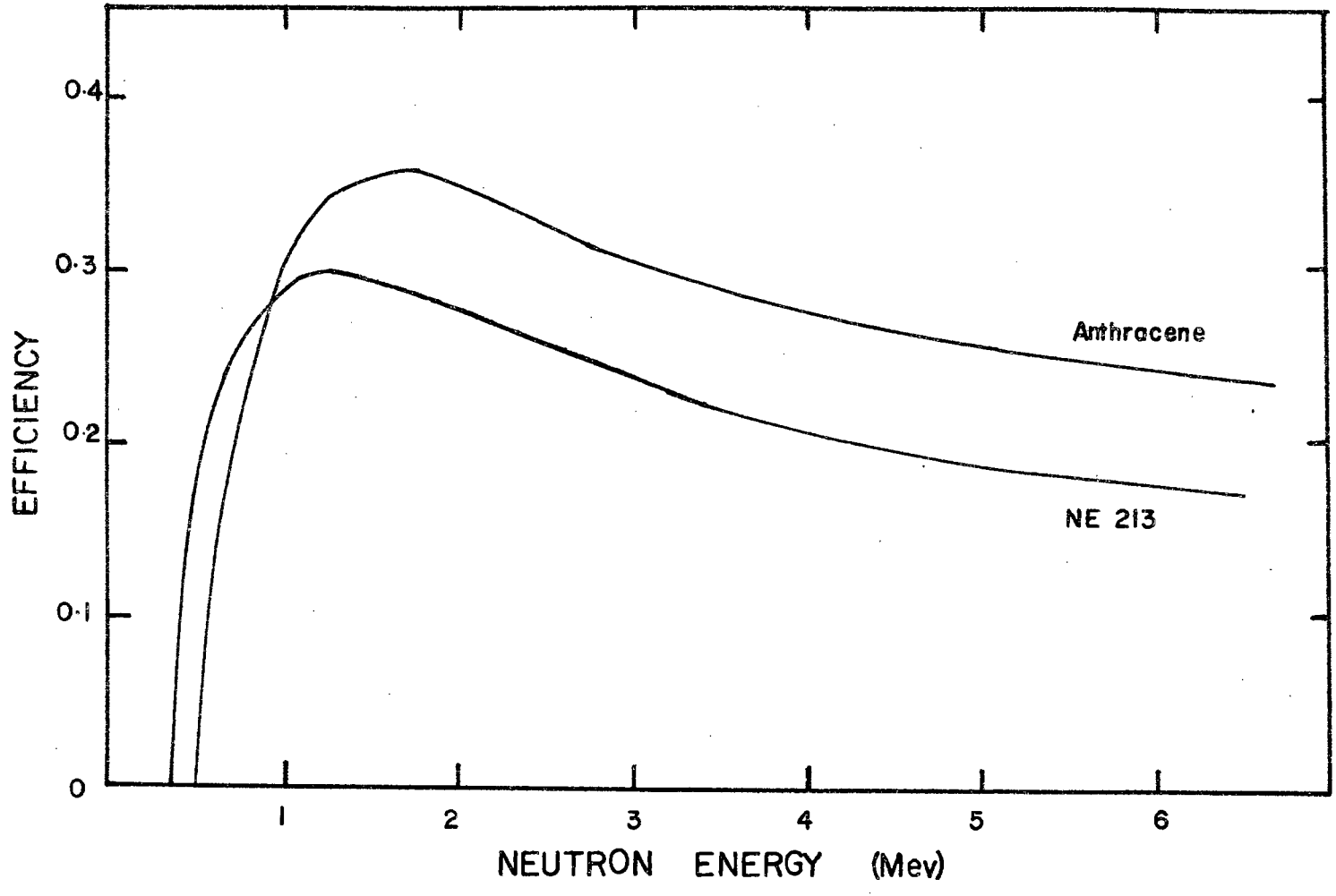

Fig. 2.6: The Absolute Efficiency Functions for the Detectors

The calculated absolute efficiency functions for the two detectors are plotted in fig. 2.6.

2.9 Description of the Runs

There were three separate series of runs of the experiment.

Run Series I

This series lasted three days and was largely of an exploratory nature. On this occasion the detectors used were not those described in section 2.2. Two NE 213 liquid scintillators were used; one mounted on a 12.5 cm diameter 58AVP photomultiplier tube, and the other on the 5 cm diameter 56AVP tube. The cradle carrying the moveable (5 cm) tube was attached to a pivot arm which was centred below the source using a plumb line. The detector-source distances were 7 cm for the 5 cm tube and 14 cm for the 12.5 cm tube. This meant that the solid angle subtended at the source was approximately equal for the two detectors. Coincidence spectra, as well as singles rates, were measured at steps of 15° over the angular range 55° to 180° between the detectors. (The detector geometry limited the minimum angular separation θ_{min} to 55°.)

Run Series II

This series lasted two days and the detecting system used was as described earlier in this chapter and illustrated in fig. 2.1. Using this detector geometry, θ_{min} was 20° for detector-source distances of 10 cm. Thirty of the thirty-six runs made in this series were at angles in the range 20° to 180° (in angular steps of 15°), at least two measurements being made at each angle. By increasing the detector-source distances to 18 cm, six runs were also made at angles in the range 12° to 20°. The runs were mostly of fifty minute duration.

Run Series III

This series, which lasted five days, was the most comprehensive of the three. This time the angular steps were 10° and the measurements were extended past 180° to check on the geometrical alignment of the system. Eighty-two runs, mostly of duration eighty minutes, were made at angles in the range 10° to 260°. As in the second run series, measurements at detector separations of greater than 20° were made with the detectors placed at a distance of 10 cm from the source. Measurements were made at smaller angular separations by increasing the detector-source distances to 18 cm.

Apart from these runs, eleven runs were also made with an Am-Be source for a variety of detector-source geometries. This source emits single neutrons and the measurements were made to investigate the likelihood of single neutrons being scattered from one detector into the other, thus appearing as a coincidence.

CHAPTER THREE

EXPERIMENTAL RESULTS

3.1 The Run Series

As already described in chapter 2, the runs consisted of the measurement of the singles rates in each detector, the coincidence rate between the two detectors and the time spectrum of the coincidences for a range of angles between the detectors. In all but a few cases the sum of the coincidences in the coincidence-time spectrum agreed closely with the scaler measurement. Several typical coincidence-time spectra obtained during run series III are plotted in fig 3.1. As illustrated in these spectra the random coincidence background was very small and could therefore safely be neglected in this series of runs. The same was also true for the first and second series of runs.

Each set of measurements extended over a period of a few days thus placing stringent demands on the stability of the electronic apparatus used. This stability was checked by monitoring the singles count rates from the two detectors as illustrated in fig 3.2 for those series III runs carried out at detector source distances $d_1 = d_2 = 10.0$ cm. The singles rates for the two detectors are plotted against run number in fig 3.2 (a). Abrupt changes are seen to have occurred in the singles count rate from the NE 213 detector at run numbers 4 and 31. A change in the count rate of the order of 5% is seen to have occurred between runs 3 and 4, while the change between runs 30 and 31 was about 10%. It is not clear what the reason for these sudden jumps was.

Two methods were devised to minimise the effects of electronic drifts on the final results. Firstly, several short runs were made at each angle in preference to one long run. By taking measurements in this way the effects of electronic drifts are more likely to be averaged out. This is illustrated by regrouping the data of fig. 3.2 (a) and plotting the singles count rate as a function of the angle of the run, shown in fig. 3.2 (b).

The second method devised was to determine the angular dependence of neutron coincidences in terms of a ratio $R(\Theta)$ which is independent of the

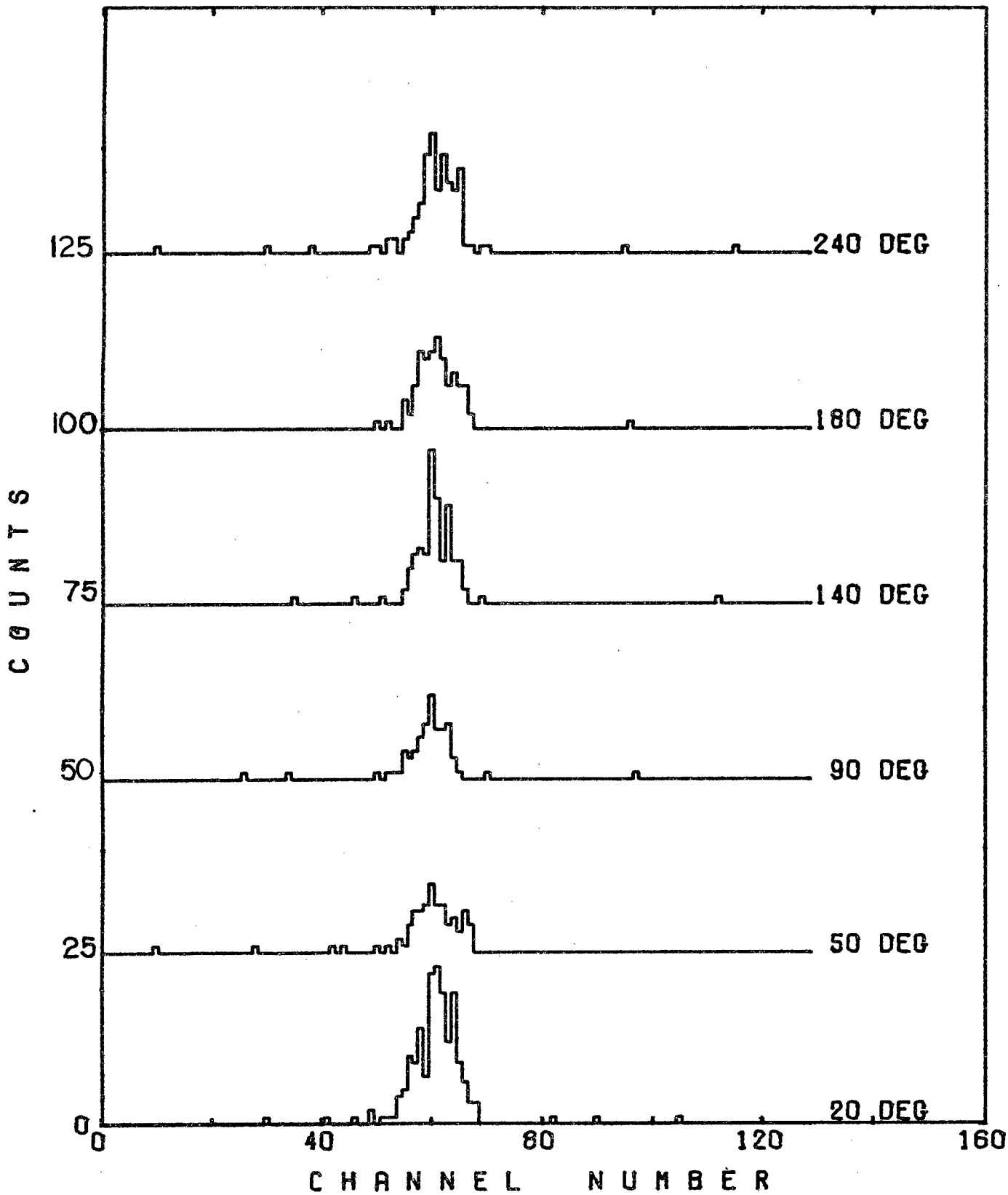

Fig. 3.1: TYPICAL CF 252 COINCIDENCE-TIME SPECTRA FROM RUN SERIES III

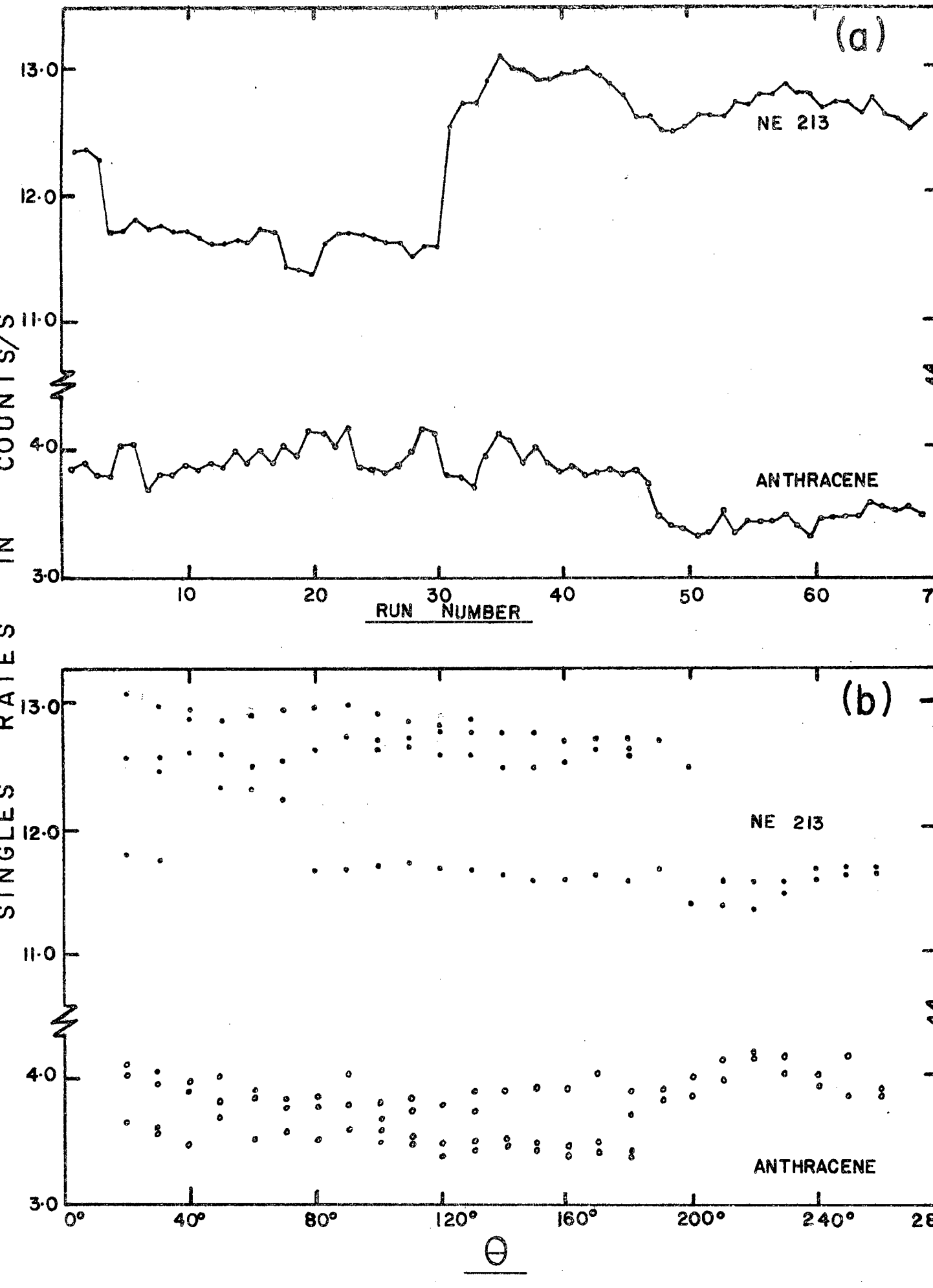

Fig. 3.2: (a) Singles rates for the two detectors vs. run number.
(b) " " " " " " " angle.

of the efficiencies of the detectors. This is shown below.

Define:

$\dot{N}_i$ = measured singles rate from detector i

$\dot{N}'_i$ = actual singles rate incident on detector i

ε_i = efficiency of detector i for an "average" fission neutron

$\dot{N}_{co}(\theta)$ = measured coincidence rate between detectors at angle θ

$\dot{N}'_{co}(\theta)$ = actual coincidence rate incident on detectors at angle θ

Then $\dot{N}_1 = k_1 \varepsilon_1 \dot{N}'_1$

$\dot{N}_2 = k_2 \varepsilon_2 \dot{N}'_2$

and $\dot{N}_{co}(\theta) = k_1 k_2 \varepsilon_1 \varepsilon_2 \dot{N}'_{co}(\theta)$

where k_1 and k_2 are constants which are determined by the geometry of the detectors.

Define:

$$R(\theta) = \dot{N}_{co}(\theta)/\dot{N}_1 \dot{N}_2$$

$$= k_1 k_2 \varepsilon_1 \varepsilon_2 \dot{N}'_{co}(\theta)/(k_1 \varepsilon_1 \dot{N}'_1)(k_2 \varepsilon_2 \dot{N}'_2)$$

Thus $R(\theta) = \dot{N}'_{co}(\theta)/\dot{N}'_1 \dot{N}'_2$

The ratio $R(\theta)$ is a measure of the probability of detecting a coincidence for two detectors at angular separation θ and it is independent of the efficiencies of the detectors. It is important to note that $R(\theta)$ is also independent of the geometry. This means that the measured value of $R(\theta)$ is independent of the detector-source distances used, a fact which was used in run series II and III for making measurements at angles of less than 20° between the detectors. For convenience, in the tabulated data $R(\theta)$ has been multiplied by a factor of 10^4 so that its value is generally between 2 and 4 seconds/count.

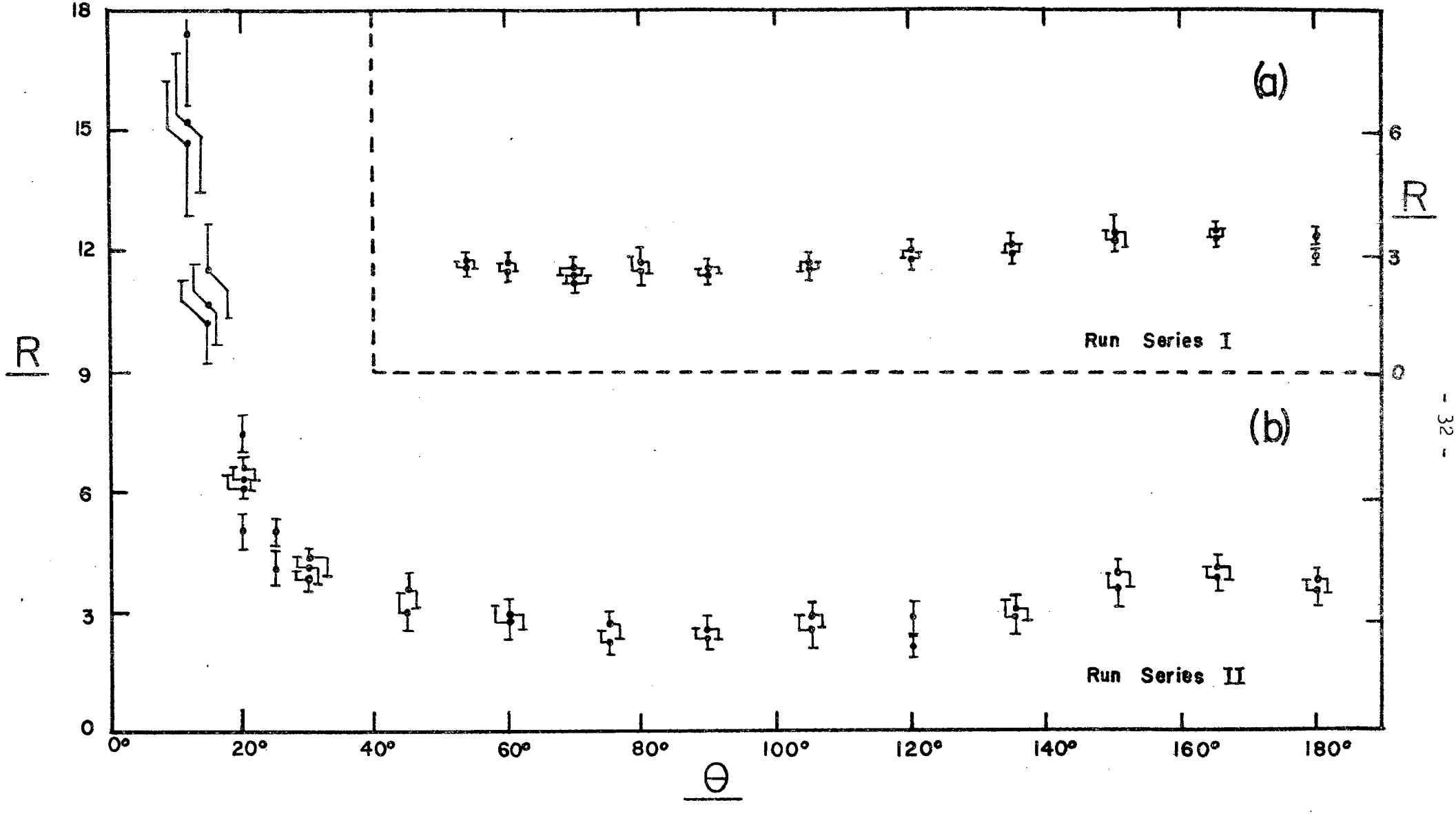

Fig. 3.3: Results of Run Series I and II

During each run series more than one run was made at each angle. The resulting values of $R(\theta)$ and their uncertainties $\Delta R(\theta)$ were combined to give a weighted mean value $\bar{R}(\theta)$ with an associated uncertainty $\Delta\bar{R}(\theta)$ at each angle. The methods used in the data reduction and the calculation of the standard deviations are described in appendix A.

3.1 The Run Series

(i) Run Series I

The results obtained in this run series are presented in table 3.1 and plotted in fig 3.3 (a) for comparison with the results of the second run series and also to show the internal consistency of the separate measurements of $R(\theta)$. The geometry of the detecting system was such that no measurements were possible at angles of less than 55°. For this series the operating biases on the detectors were not determined and the results obtained cannot therefore be compared directly with the computer simulation of the experiment (described in chapter 4).

(ii) Run Series II

As in the first series the operating biases of the detectors were not determined in this case. The results of this series are presented in table 3.2 and plotted in fig 3.3 (b). The outstanding feature of the results is the strong peaking of the coincidence ratio $R(\theta)$ at small angles θ between the detectors. Fig 3.3 (b) shows that, as for the results of the first run series, the separate measurements of $R(\theta)$ at each θ are internally consistent.

(iii) Run Series III

This series was the most comprehensive of the three and, for the first time, measurements were made at angles beyond 180° to test for

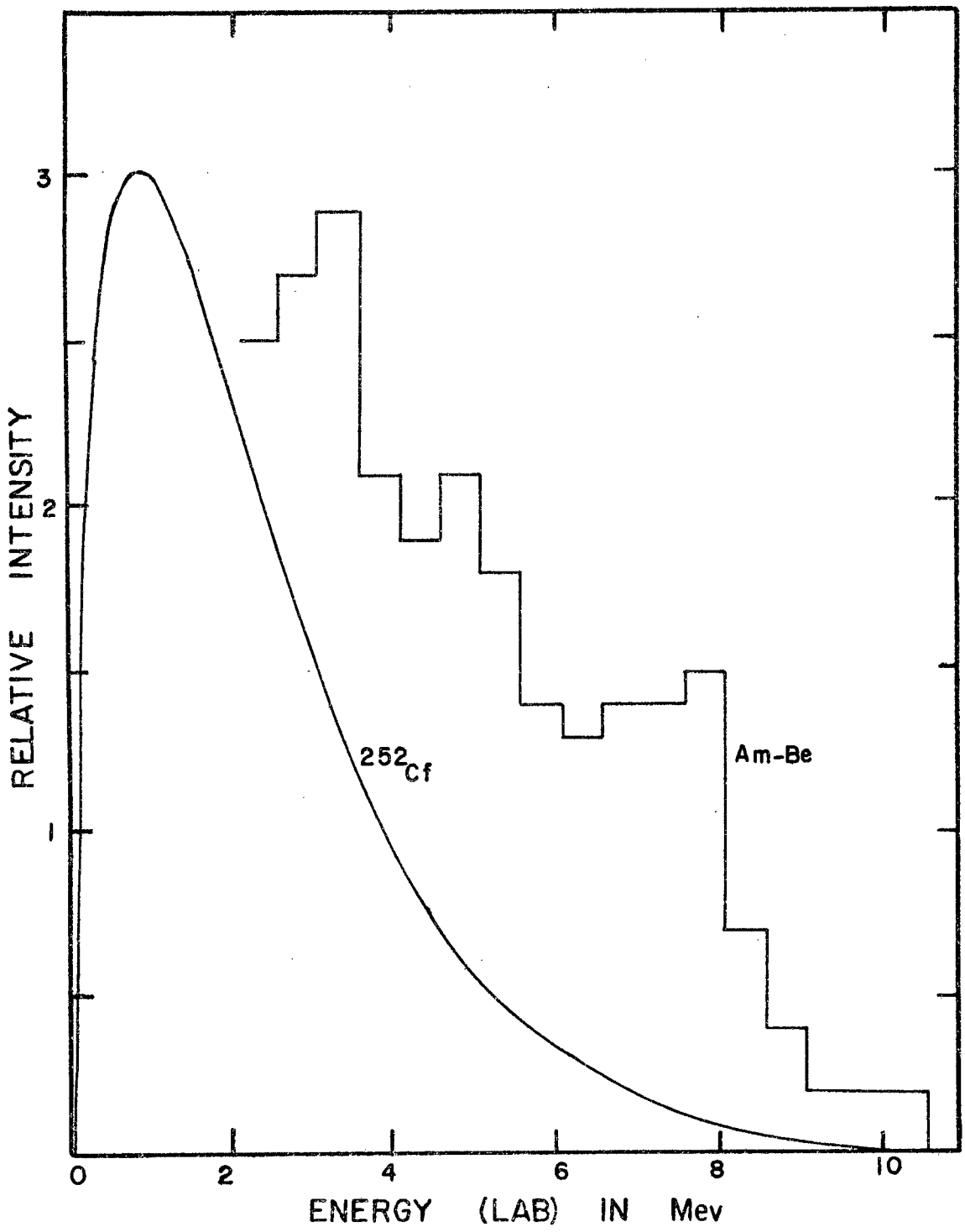

Fig. 3.4: Neutron Energy Spectra
The Am-Be spectrum is that measured by Lorch (Lo 73)
(No measurements were made below 2 Mev)
The ^{252}Cf spectrum has been represented by the Watt distribution

geometrical symmetry. The operating biases of the detectors were determined as described in chapter 2, and the results of the runs are therefore directly comparable with the predictions of the computer simulation of the experiment.

From the results obtained in run series II it was apparent that more information was needed at small angular separations. In particular it was important to determine whether the peak observed at small angles was due to fission neutron pairs, or whether it could perhaps have arisen from single neutrons scattering from one detector to the other, thereby being detected in both detectors. For this purpose several runs were made for a variety of detector configurations using an Am-Be source which emits single neutrons. This gave a direct measurement of the proportion of coincidences arising from scattering of single neutrons since all "true" coincidences registered using this source are necessarily the result of such interactions.

The tests with the Am-Be source were made at seven angles in the range 0° to 90°, and for a variety of source-detector geometries in the case of $\theta = 15^{\circ}$. The results are given in table 3.4. The singles coincidence rate increases, as would be expected, for small values of θ. However for all detector configurations and for all angles θ the values of $R(\theta)$ obtained from the Am-Be runs are extremely small compared with the corresponding values obtained in the ^{252}Cf runs.

The energy spectra of the neutrons emitted from the Am-Be source and those emitted in ^{252}Cf spontaneous fission are quite different (see fig.3. In view of this the Am-Be measurements of the scattering effect cannot be expected to give an accurate correction to the value of $R(\theta)$ at small angles θ . However it can be assumed that the Am-Be data overestimates

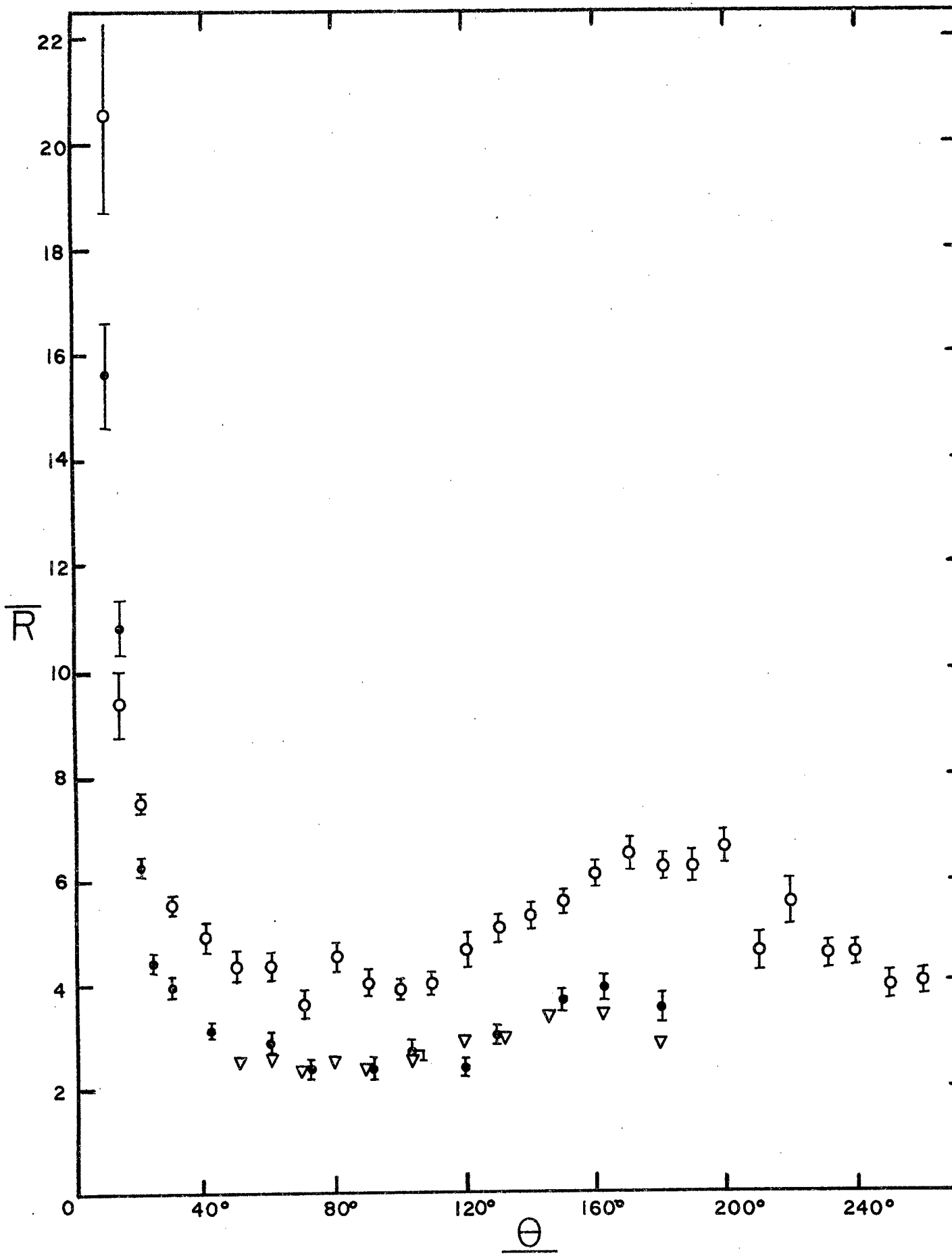

Fig. 3.5: Results of the Three Run Series
Triangle: Run Series I (Uncertainties smaller than point sizes)
Solid : Run Series II
Circle : Run Series III

this correction since the neutrons emitted from this source have a considerably higher mean energy than the ^{252}Cf fission neutrons. As a result these neutrons have a larger probability of depositing sufficient energy in each detector to be detected in both, thus appearing as a coincidence.

As a further check on the effects of scattering, ^{252}Cf measurements were made at three different detector-source distances for a detector separation of 20° and at two distances at 15°. For a fixed angular separation the solid angle of one detector subtended at the other detector decreases rapidly with increasing distance from the source. As a result, the proportion of neutrons scattered from one detector to the other will decrease, leading to a decrease in the value of $R(\theta)$ if the false coincidences form a large component of the total value of $R(\theta)$. Examination of the ^{252}Cf data at 15° and 20° shows that the values of $R(\theta)$ obtained using different detector-source distances agree well within experimental error, thereby confirming that the scattering background must be small.

In the light of the evidence presented above, no corrections were made to the data for coincidences arising from the scattering of single neutrons. The data obtained in run series III are presented in table 3.3. Examination of these data shows that, as in the first two run series, the separate measurements of $R(\theta)$ at each θ are generally internally consisten

In fig. 3.5 the mean values $\bar{R}(\theta)$ and their uncertainties $\Delta\bar{R}(\theta)$ measured in the three series of runs are plotted. All three sets of data are seen to show the same general features although the values of $\bar{R}(\theta)$ measured during the third series are consistently higher than those of the other two series.

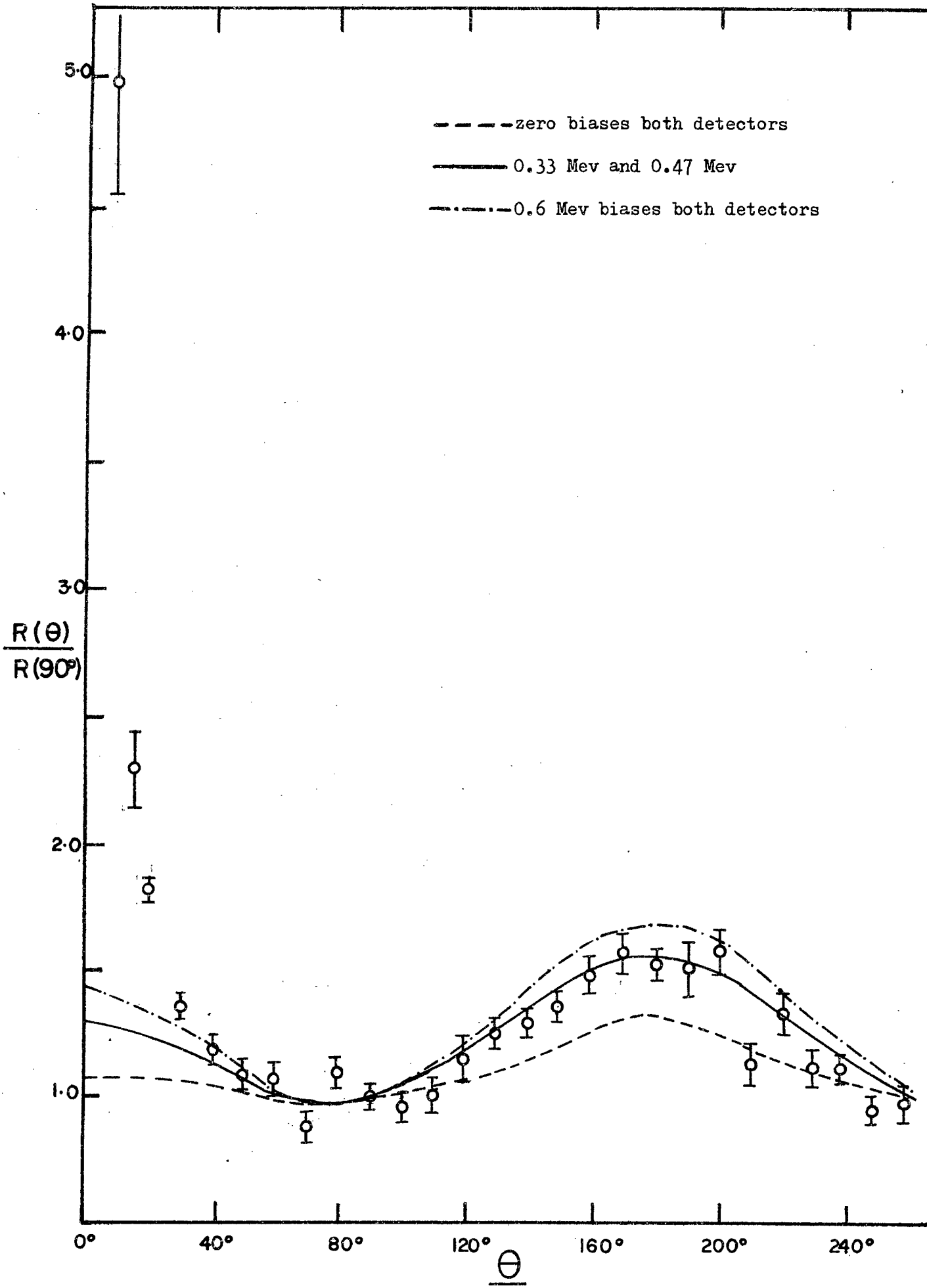

Fig. 3.6: Normalised coincidence ratio R(θ) from Run Series III (circles) The curves represent the predicted n-n angular correlation for different bias levels (all normalized at $\theta = 90^{\circ}$)

From its definition, $R(\theta)$ should be insensitive to the detector efficiencies ε_1 and ε_2 and as a result we expect it to be the same for all three sets of data. The fact that this is not so is thought to be due to different gamma-rejection efficiencies of the detecting systems used in the three run series. In particular, in run series III (for which the PSD rejection system was especially carefully set) the values obtained for $R(\theta)$ were higher than in either of the other run series. This would be expected since a larger gamma breakthrough (even though still less than about 0.05%) would tend to increase $\dot{N}_1$ and $\dot{N}_2$ far more rapidly than $\dot{N}_{co}$.

The measurements of the coincidence ratio $R(\theta)$ obtained in run series III are used exclusively from this point on since they are the only measurements that are directly comparable with the results obtained from the computer simulation of the experiment. In order to compare these data with the results of the computer simulation, the values of $R(\theta)$ were normalized to unity at $\theta = 90^{\circ}$. This normalized distribution is plotted in fig. 3.6 together with three computer generated distributions of $R(\theta)$ corresponding to different detector bias levels.

Table 3.1: Results of Run Series I

θ	Run No.	Live Time (Sec)	N_1	N_2	N_{co}	R	ΔR	$\bar{R}$	$\Delta\bar{R}$
55°	3	10000	329730	140922	1182	2.54	0.08	2.53	0.07
	22	3410	108912	45083	362	2.51	0.14		
60°	4	10000	330017	139123	1188	2.59	0.08	2.56	0.07
	18	3493	113871	45033	364	2.48	0.13		
70°	6	3677	128167	49389	388	2.25	0.12	2.39	0.07
	12	3447	117751	57365	489	2.50	0.12		
	23	3414	114224	46327	376	2.43	0.13		
80°	11	3435	119092	53384	488	2.64	0.12	2.51	0.08
	13	3567	121297	61499	502	2.40	0.11		
90°	5	10000	339787	141628	1158	2.41	0.07	2.41	0.06
	14	3563	121102	57069	465	2.40	0.11		
105°	10	3657	121414	49855	413	2.50	0.13	2.50	0.09
	19	3445	113878	47709	392	2.49	0.13		
120°	2	10000	337602	149688	1431	2.83	0.08	2.80	0.07
	15	3606	121653	58425	537	2.72	0.12		
135°	7	3763	129586	50506	499	2.87	0.13	2.94	0.09
	17	3670	120788	48818	486	3.02	0.14		
150°	8	3632	130543	47770	568	3.31	0.14	3.31	0.10
	21	3448	113295	46499	507	3.32	0.15		
165°	9	3768	134530	49971	605	3.39	0.14	3.35	0.10
	20	3439	114452	45577	501	3.30	0.15		
180°	1	10000	384309	178655	1986	2.89	0.07	2.98	0.06
	16	3697	124210	54895	613	3.32	0.14		

NOTE: All runs at d_1 = 7.0 cm, d_2 = 14.0 cm.

Table 3.2: Results of Run Series II

θ	Run No.	Live Time (Sec)	N_1	N_2	N_{co}	R	ΔR	$\bar{R}$	$\Delta\bar{R}$
(a)	34	3170	8014	18837	83	17.43	1.91		
12°	35	3423	8597	20111	77	15.24	1.74	15.66	1.03
	36	3330	8256	19844	72	14.63	1.72		
(b)	31	3111	12605	30165	130	10.64	0.93		
15°	32	3084	12450	30111	124	10.20	0.92	10.75	0.54
	33	3132	12385	31053	141	11.48	0.97		
(c)	1	3092	23809	57240	278	6.31	0.38		
	2	3084	23457	56486	320	7.45	0.42		
20°	25	3151	23507	58730	280	6.39	0.38	6.21	0.17
	27	3090	22907	57309	216	5.08	0.35		
	30	3091	23150	57858	271	6.25	0.38		
25°	28	3088	23041	57494	177	4.13	0.31	4.46	0.23
	29	3097	22959	57303	206	4.85	0.34		
	3	3110	23452	57006	182	4.23	0.31		
30°	24	3147	23048	58081	161	3.78	0.30	3.99	0.18
	26	3162	22714	58604	164	3.90	0.30		
45°	4	3051	22449	55572	120	2.93	0.27	3.15	0.19
	23	3287	23754	60006	147	3.39	0.28		
60°	5	3055	22607	55964	115	2.78	0.26	2.79	0.18
	22	3521	25087	64336	128	2.79	0.25		

NOTE: (a) For runs at $\theta = 12^\circ$ $d_1 = d_2 = 18.0$ cm.

(b) For runs at $\theta = 15^\circ$ $d_1 = d_2 = 14.0$ cm.

(c) For runs at $\theta \geq 20^\circ$ $d_1 = d_2 = 10.0$ cm.

Table 3.2 (cont.)

θ	Run No.	Live Time (Sec)	N_1	N_2	N_{co}	R	ΔR	$\bar{R}$	$\Delta\bar{R}$
75^o	6	3061	22704	55906	93	2.24	0.23	2.42	0.17
	21	3298	24001	60302	116	2.64	0.25		
90^o	7	3061	22901	55922	98	2.34	0.24	2.40	0.17
	20	3213	23554	58366	105	2.45	0.24		
105^o	8	3052	22617	57076	116	2.74	0.25	2.62	0.18
	19	3106	22396	56674	102	2.50	0.25		
120^o	9	3073	22612	57837	90	2.13	0.22	2.39	0.17
	18	3253	24046	60197	121	2.72	0.25		
135^o	10	3064	22800	57519	123	2.87	0.26	2.89	0.18
	17	3143	23249	58529	126	2.91	0.26		
150^o	11	3060	22508	57302	144	3.42	0.28	3.61	0.20
	16	3128	23257	58673	167	3.83	0.30		
165^o	12	3082	23206	57250	175	4.09	0.31	3.86	0.21
	15	3128	22946	58053	156	3.66	0.29		
180^o	13	3080	22754	57093	146	3.46	0.29	3.53	0.20
	14	3101	22906	57628	153	3.59	0.29		

Table 3.3: Results of Run Series III

θ	Run No.	d_1 (cm)	d_2 (cm)	Live Time (Sec)	N_1	N_2	N_{co}	R	ΔR	$\bar{R}$	$\Delta\bar{R}$
10°	83	18.0	18.0	6419	8903	28176	80	20.47	2.29	20.51	1.81
	86	"	"	3893	5283	17198	48	20.57	2.97		
15°	75	14.0	14.0	3830	7763	24674	46	9.20	1.36	9.44	0.67
	76	"	"	5646	11041	35703	64	9.17	1.15		
	88	"	"	3856	8093	26695	58	10.35	1.36		
	90	18.0	18.0	6151	8329	26120	32	9.05	1.60		
20°	6	10.0	10.0	57401	233030	679290	2099	7.61	0.17	7.51	0.15
	35	"	"	3831	15927	50307	177	8.46	0.64		
	73	"	"	6529	23900	82461	188	6.23	0.45		
	89	14.0	14.0	3849	8131	26203	42	7.59	1.17		
	84	18.0	18.0	3859	5129	16574	22	9.99	2.13		
30°	16	10.0	10.0	24968	99825	294419	674	5.73	0.22	5.56	0.18
	36	"	"	3833	15734	49935	104	5.07	0.50		
	72	"	"	5305	18968	66344	136	5.73	0.49		
	74	"	"	3580	12912	45174	80	4.91	0.55		
40°	34	10.0	10.0	11504	45746	148911	298	5.03	0.29	4.89	0.22
	37	"	"	3835	15085	49830	102	5.20	0.52		
	71	"	"	5444	19096	68983	106	4.38	0.43		
50°	1	10.0	10.0	4797	18472	59407	103	4.50	0.44	4.47	0.27
	38	"	"	3827	15433	49442	88	4.41	0.47		
	70	"	"	3835	14038	48550	80	4.50	0.50		
60°	2	10.0	10.0	4795	18500	59297	120	5.25	0.48	4.48	0.50
	39	"	"	4453	17423	57688	106	4.70	0.46		
	69	"	"	3837	13491	48201	60	3.54	0.46		

Table 3.3 (cont.)

θ	Run No.	d_1 (cm)	d_2 (cm)	Live Time (Sec)	N_1	N_2	N_{co}	R	ΔR	$\bar{R}$	$\Delta\bar{R}$
70°	3	10.0	10.0	4800	18355	59021	88	3.90	0.42	3.68	0.24
	40	"	"	4616	17704	59986	82	3.56	0.39		
	68	"	"	3841	13747	48446	62	3.58	0.45		
80°	4	10.0	10.0	4797	18273	56228	108	5.04	0.49	4.57	0.27
	41	"	"	4493	17408	58419	98	4.33	0.44		
	67	"	"	3865	13671	48975	76	4.39	0.50		
90°	5	10.0	10.0	21122	85701	247813	410	4.08	0.20	4.13	0.17
	42	"	"	4643	17704	60488	102	4.42	0.44		
	66	"	"	3840	13715	49145	72	4.10	0.48		
100°	7	10.0	10.0	4872	17935	57239	67	3.18	0.39	3.97	0.15
	43	"	"	24859	95047	322570	488	3.96	0.18		
	63	"	"	4271	15002	54557	98	5.11	0.52		
	65	"	"	3944	14232	49965	78	4.33	0.49		
110°	8	10.0	10.0	4799	18023	56533	91	4.29	0.45	4.11	0.23
	44	"	"	3840	14814	49584	96	5.02	0.51		
	62	"	"	3909	13648	49685	54	3.11	0.42		
	64	"	"	3847	13500	49177	77	4.46	0.51		
120°	9	10.0	10.0	4804	18190	56377	102	4.78	0.47	4.70	0.29
	45	"	"	4048	13253	51957	76	4.47	0.51		
	60	"	"	3978	13462	51053	84	4.86	0.53		
130°	10	10.0	10.0	4805	18605	56408	94	4.30	0.44	5.16	0.25
	47	"	"	3917	14658	49601	117	6.30	0.58		
	59	"	"	4234	14532	54666	92	4.90	0.51		
	61	"	"	4367	15165	55987	112	5.76	0.54		

Table 3.3 (cont.)

θ	Run No.	d_1 (cm)	d_2 (cm)	Live Time (Sec)	N_1	N_2	N_{co}	R	ΔR	$\bar{R}$	$\Delta \bar{R}$
140°	11	10.0	10.0	6923	26654	80958	167	5.36	0.41	5.31	0.25
	49	"	"	4194	14420	52582	106	5.86	0.57		
	58	"	"	8288	29122	106190	188	5.04	0.37		
150°	12	10.0	10.0	5280	20800	61480	142	5.86	0.49	5.65	0.27
	50	"	"	7861	26838	98564	180	5.35	0.40		
	57	"	"	4227	14604	54219	112	5.98	0.56		
160°	13	10.0	10.0	4796	18576	55868	134	6.19	0.53	6.10	0.26
	51	"	"	5441	18209	68471	156	6.81	0.55		
	56	"	"	13521	46681	172613	348	5.84	0.31		
170°	14	10.0	10.0	4993	20121	58337	140	5.96	0.50	6.49	0.33
	53	"	"	4185	14738	53098	128	6.85	0.61		
	55	"	"	3974	13737	50770	122	6.95	0.63		
180°	15	10.0	10.0	4803	18735	55901	124	5.69	0.51	6.30	0.23
	33	"	"	4796	17833	61221	147	6.46	0.53		
	52	"	"	14671	49504	186039	414	6.60	0.32		
	54	"	"	3872	13075	49064	98	5.91	0.60		
190°	17	10.0	10.0	4795	18561	56253	136	6.25	0.54	6.24	0.37
	32	"	"	4781	18113	60948	144	6.24	0.52		
200°	18	10.0	10.0	4793	19344	54925	138	6.23	0.53	6.57	0.38
	31	"	"	4793	18369	60248	160	6.93	0.55		
210°	19	10.0	10.0	5273	20891	60244	118	4.94	0.46	4.69	0.32
	30	"	"	4794	19850	55701	103	4.47	0.44		

Table 3.3 (cont)

θ	Run No.	d_1 (cm)	d_2 (cm)	Live Time (Sec)	N_1	N_2	N_{co}	R	ΔR	$\bar{R}$	$\Delta\bar{R}$
220°	20	10.0	10.0	4918	20619	56046	129	5.49	0.48	5.55	0.34
	29	"	"	5246	21935	60946	143	5.61	0.47		
230°	21	10.0	10.0	5744	23940	66927	118	4.23	0.39	4.57	0.30
	28	"	"	4801	19492	55410	114	5.07	0.47		
240°	22	10.0	10.0	9933	40216	116385	202	4.29	0.30	4.59	0.26
	27	"	"	4789	18636	55773	118	5.44	0.50		
250°	23	10.0	10.0	7470	31093	87547	148	4.06	0.33	3.95	0.25
	26	"	"	5728	21900	66818	97	3.80	0.39		
260°	24	10.0	10.0	10268	39780	120377	178	3.82	0.29	4.05	0.24
	25	"	"	4800	18502	56067	100	4.63	0.46		

Table 3.4: Am-Be Data - Run Series III

θ	Run No.	d_1 (cm)	d_2 (cm)	Live Time (Sec)	N_1	N_2	N_{co}	R	ΔR	$\bar{R}$	$\Delta\bar{R}$
10°	87	18.0	18.0	1473	137698	385874	1312	0.36	0.01	0.36	0.01
	77	14.0	14.0	1404	207935	571920	1011	0.12	0.01	0.12	0.01
	82	"	"	1412	216213	608878	1086	0.12	0.01		
15°	91	18.0	18.0	730	64900	179499	172	0.11	0.01	0.11	0.01
	78	24.0	14.0	1403	73772	566250	634	0.21	0.01	0.20	0.01
	79	"	"	1392	73047	573260	554	0.18	0.01		
20°	85	18.0	18.0	1485	129055	362670	220	0.07	0.01	0.07	0.01
30°	93	14.0	14.0	1082	160309	457638	208	0.03	0.00	0.03	0.00
45°	81	14.0	14.0	1426	204169	595046	110	0.01	0.00	0.01	0.00
60°	92	14.0	14.0	1070	149156	439180	70	0.01	0.00	0.01	0.00
90°	80	14.0	14.0	1378	208841	595815	77	0.01	0.00	0.01	0.00

CHAPTER FOUR

THE COMPUTER SIMULATION OF ^{252}Cf FISSION NEUTRON EMISSION

4.1 Sampling with Random Numbers

4.2 The Monte Carlo Programme

The technique used to simulate neutron emission in ^{252}Cf spontaneous fission was the Monte Carlo method (Ca 59, Sh 66) which is aptly described as "playing a game of chance to imitate nature". In this particular case the fission process was simulated step-by-step, the behaviour of the "fissioning nucleus" and the subsequent "fission fragments" being selected in a random manner from the existing possibilities according to the evaporation model. During the selection process the choices to be made were weighted according to the experimentally observed probability of their occurrence. "Prompt neutrons" evaporated from "fission fragments" were tracked and the probability of their detection by "detectors" having the same properties as those used in the actual experiment were determined. Only binary fissions (i.e. resulting in the formation of two fragments) were considered in the calculation, and scission neutrons were ignored. The first assumption is justified by the fact that ternary fission of ^{252}Cf is very rare (about 1 in 300 fissions). The contribution of scission neutrons is also expected to be small. Their contribution will be considered in more detail in chapter 5.

4.1 Sampling with Random Numbers

A Monte Carlo programme needs to have on call a source of random numbers equidistributed on the interval $[0,1]$. The Lehmer generator (Mi 68) which generates a cycle of pseudorandom numbers of length $2^{35} - 32$ (for the UNIVAC 1106 system) from a specified starting integer was used for this purpose. A useful feature of the Lehmer generator is that the same sequence of random numbers is always generated from the same starting integer. This means that if the same starting integers are used in a set of calculations differing only in their initial input parameters, any statistical fluctuations (which would arise if different random numbers were used) in the results are eliminated.

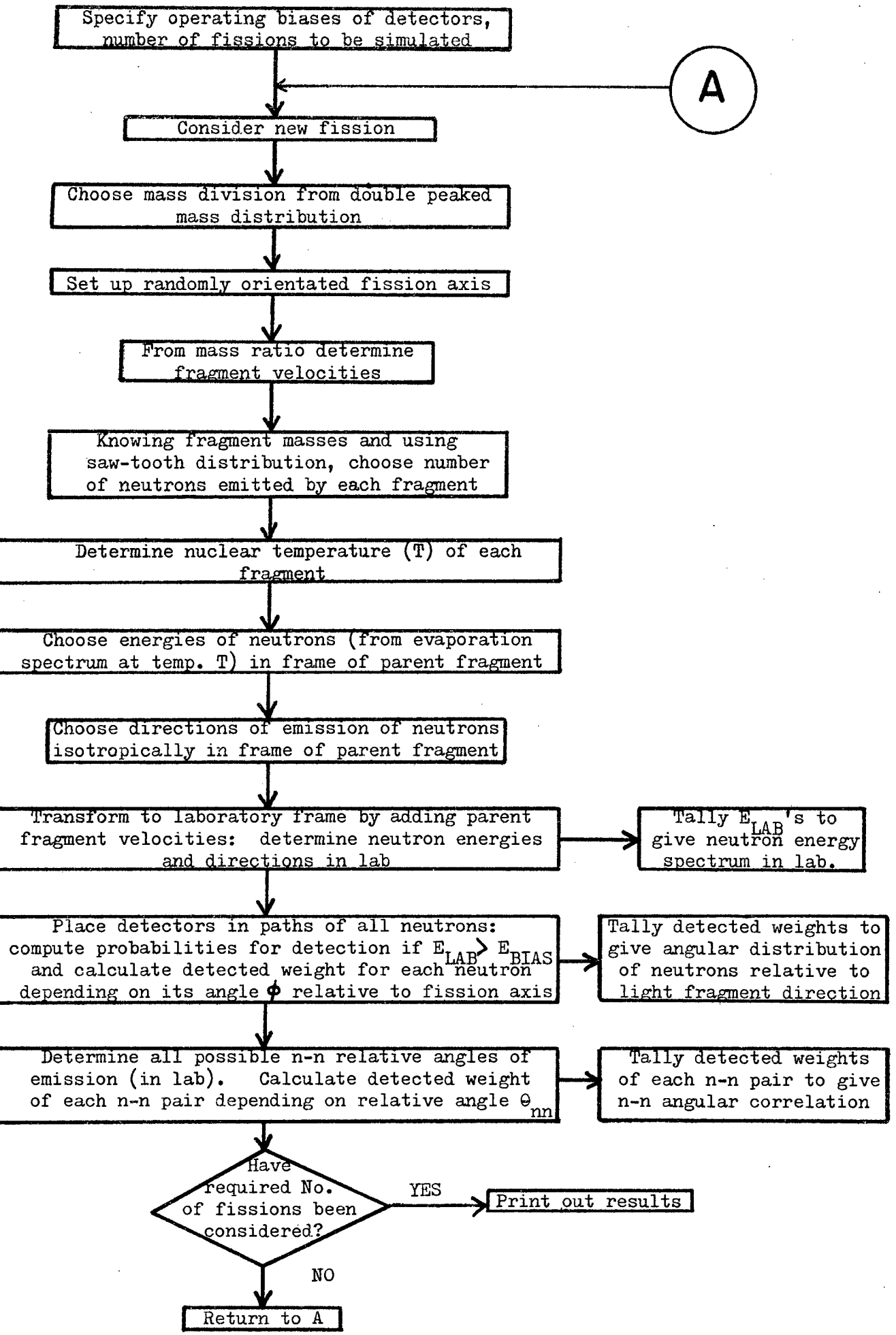

Fig. 4.1: Flow Diagram of the Monte Carlo Programme

By using random numbers it is possible to sample from any distribution. The method used is called the rejection technique (Ca 59) and it applies to distributions with a finite range, say $0 \leq x \leq a$. If L is the maximum value of F(x) then the sampling procedure is:

(i) Select two random numbers R_1 and R_2

(ii) If $LR_1 \leq F(aR_2)$, then choose aR_2 as a random variate from F(x)

(iii) If $LR_1 > F(aR_2)$, reject the pair R_1 and R_2 and repeat the process with new pairs of random numbers until (ii) is satisfied.

4.2 The Monte Carlo Programme

A flow diagram showing the basic steps in the Monte Carlo simulation of the experiment is given in fig. 4.1 and the actual FORTRAN programme used is listed in appendix B. The main steps in the programme are now discussed.

(i) The Fragments

For each fission the mass (before neutron emission) of the light fragment is chosen randomly from a distribution which is specified in the programme by means of a data statement. This mass distribution, shown in fig. 4.2, consists of the mean values of the percentage yield of each mass in the range 80 amu to 126 amu obtained from nine independent determinations carried out by: Whetstone (Wh 63), Milton and Fraser (Mi 58), Fraser et al (Fr 63), Nardi and Fraenkel (Na 70), Balagna et al (Ba 71), Glendenin et al (Gl 65), Stein (St 65), Schmitt et al (Sc 66) and Mehta et al (Me 73).

The choice of the light fragment mass automatically fixes the heavy fragment mass since the pre-neutron emission mass distribution is

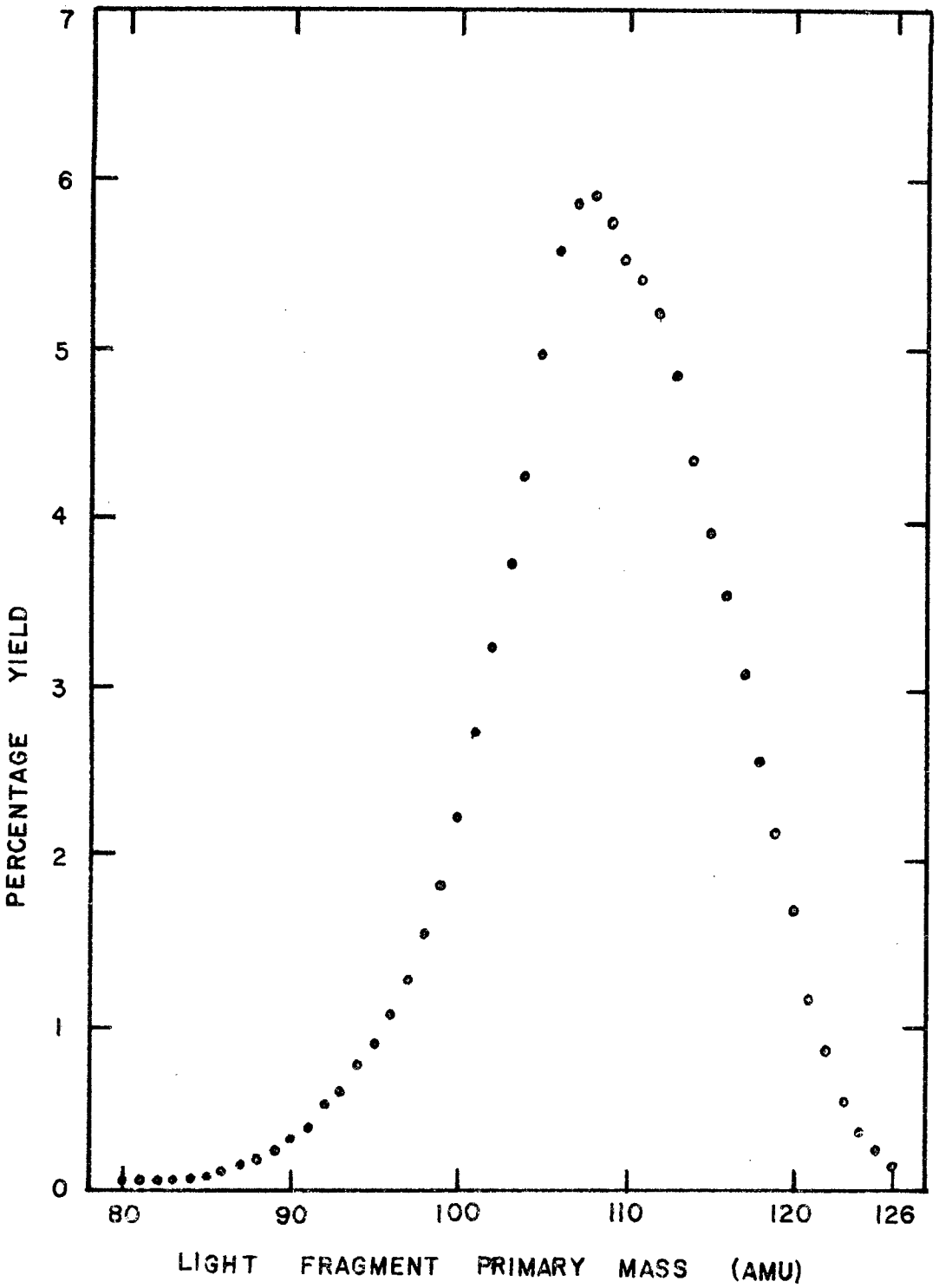

Fig. 4.2: The Light Fragment Primary Mass Distribution used in the Monte Carlo Programme

necessarily symmetric about mass number 126 for ^{252}Cf binary fission. Having chosen the fragment masses, a randomly orientated fragment axis is set up by randomly selecting three direction cosines U, V and W to specify a line in space. Then the velocities of the two fragments are determined by using Whetstone's (Wh 63) experimental data for ^{252}Cf on the fragment average velocities as a function of their mass.

(ii) Neutron Emission

(a) Number of Neutrons Emitted

The number of neutrons emitted by each fragment is chosen using the knowledge of the fragment masses and the saw-tooth neutron yield curve for ^{252}Cf. For each fragment of mass A the average number of neutrons emitted ($\bar{\nu}_A$) and the variance of this number ($\sigma^2_{\nu_A}$) is determined from the data of Signarbieux et al (Si 72). Then the actual number of neutrons emitted by each fragment is chosen randomly from a Gaussian distribution having mean $\bar{\nu}_A$ and variance $\sigma^2_{\nu_A}$. As a check on the calculation, the number of neutrons emitted by each fragment (ν_A) as well as the total number of neutrons emitted in each fission ($\nu_T = \nu_A + \nu_{252-A}$) is tallied.

From a sample of 40000 simulated fissions the average number of neutrons emitted by the light and heavy fragments and by the fission-nucleus as a whole were found to be:

$$\bar{\nu}_{LIGHT} = 2.009 \pm 0.007$$

$$\bar{\nu}_{HEAVY} = 1.736 \pm 0.007$$

$$\bar{\nu}_{TOTAL} = 3.745 \pm 0.009$$

These figures show that, on average, 15.7% more neutrons are emitted by the light fragment than by the heavy fragment in the simulated fissions. This agrees well with the value of 16% calculated by

Bowman et al (Bo 62) from their study of neutron emission in ^{252}Cf spontaneous fission. The value of $\bar{\nu}_{TOTAL}$ obtained in the simulation is in close agreement with the value of 3.743 ± 0.016 recommended by Hanna et al (Ha 69) in their review of the measurements of $\bar{\nu}$ carried out prior to 1969 for ^{252}Cf spontaneous fission.

(b) Neutron Centre-of-Mass Energies

The neutron energies E_{cm} in the frames of their parent fragments are sampled from an "evaporation" spectrum of the form proposed by Weisskopf (We 37) and given by:

$$\phi(E_{cm}) = \frac{E_{cm}}{T^2} \exp(-E_{cm}/T) \qquad (1)$$

where T is the nuclear temperature in Mev of the fragment emitting the neutron. The value of T (which is a function of the fragment mass) is determined for each fragment by making use of the fact that the average energy of the evaporation spectrum is:

$$\bar{E}_{cm} = 2T \qquad (2)$$

if no upper limit is placed on the energy (Te 59). The distribution of $\bar{E}_{cm}$ as a function of fragment mass has been measured for ^{252}Cf by Bowman et al (Bo 62) and also calculated by Kluge and Lajtai (Kl 68), with excellent agreement. The distribution of Kluge and Lajtai covers a larger mass range (from 80 to 172 amu) and it is their distribution that is used to determine $\bar{E}_{cm}$ and hence, using eqn. (2), the nuclear temperature T of the fragment. The emission energies of the neutrons in the frame of their parent fragment are

then chosen randomly from an evaporation spectrum (eqn. (1)) at temperature T.

(c) Direction of Emission of Neutrons

In accordance with the evaporation model, neutrons are assumed to be emitted isotropically in the frame of their parent fragment. This means that the neutron flux incident on a sphere surrounding the parent fragment is uniformly distributed over the surface of the sphere. To satisfy this condition, the angles (ϕ_{cm}) of emission of the neutrons relative to the fission axis (defined by the fragment directions) are chosen randomly from a sin (ϕ_{cm}) distribution while the azimuthal angles (χ) of emission are sampled from a uniform distribution on $[-\pi, \pi]$. In the transformation from the fragment frame to the laboratory frame the angle ϕ_{cm} is modified by the fragment motion while the azimuthal angle χ is the same in both frames.

(d) Transformation to the Laboratory Frame

The transformation from the fragment frame to the laboratory frame is carried out using the equations:

$$V_L^2 = V_F^2 + V_N^2 + 2V_F V_N \cos(\phi_{cm}) \qquad (3)$$

and

$$V_N^2 = V_L^2 + V_F^2 + 2V_L V_F \cos(\phi_{LAB}) \qquad (4)$$

where

V_N = Neutron velocity in fragment frame

V_L = Neutron velocity in laboratory frame

V_F = Fragment velocity in laboratory frame

ϕ_{cm} = Angle of emission in fragment frame of neutron relative to fragment direction

ϕ_{LAB} = Angle in laboratory frame between neutron and parent fragment directions.

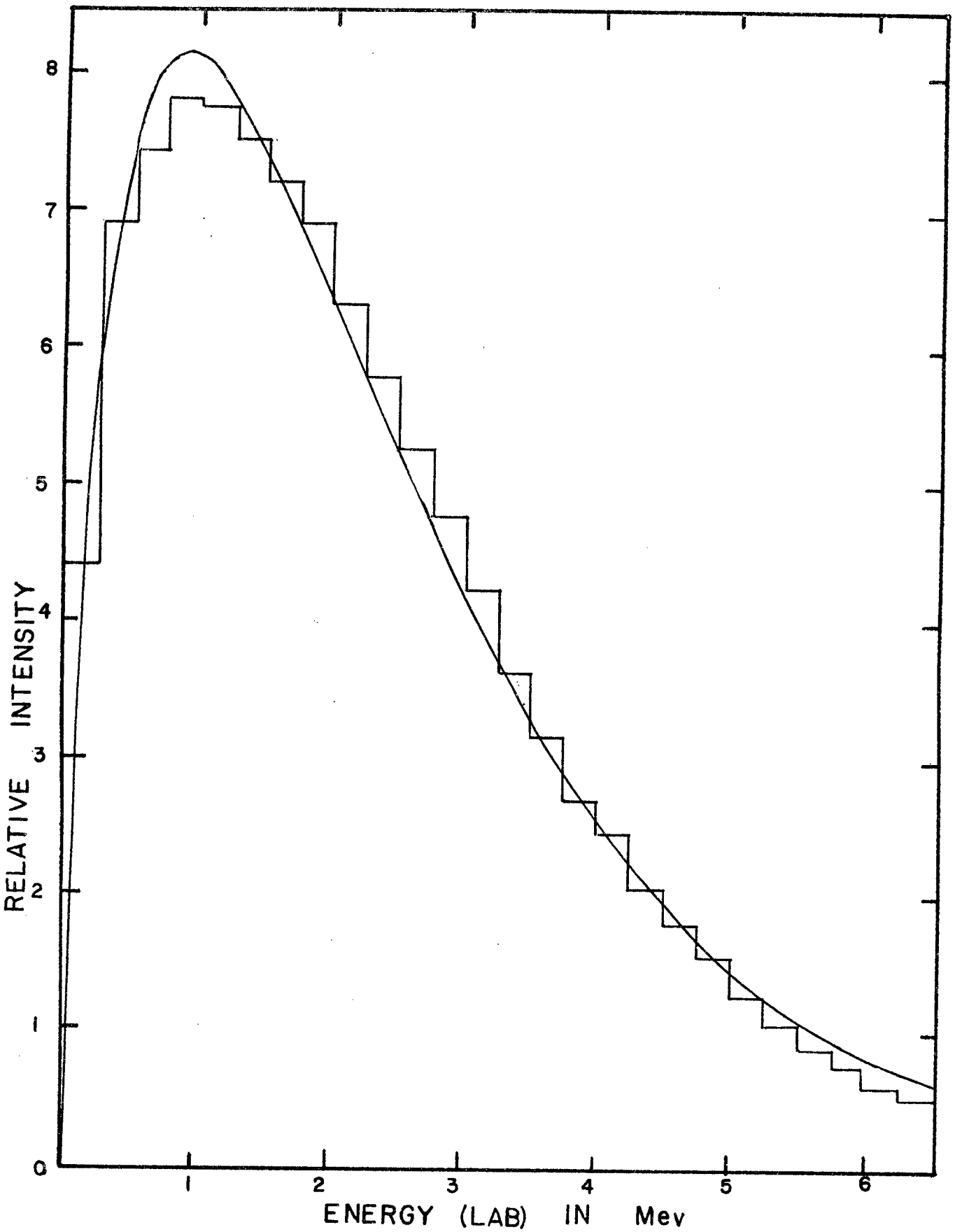

Fig. 4.3: ^{252}Cf Neutron Energy Spectrum obtained from 40000 simulated fissions (Histogram)

The smooth curve is the Watt distribution

The two distributions have been normalised to integrate to the same value.

Equation (3) is used to calculate the (laboratory) neutron energies which are tallied to yield the fission neutron energy spectrum. This spectrum, obtained from a sample of 40000 simulated fissions (i.e. about 150000 neutrons), is shown in fig. 4.3 as a histogram. Also plotted in fig. 4.3 is the Watt distribution which is generally used to represent the ^{252}Cf neutron energy spectrum (Am 72). This distribution has the form

$$N(E) = 0.373\ e^{-0.88E}\ \sinh(2.0E)^{\frac{1}{2}}$$

where N(E) is the fraction of neutrons per unit energy range and E is the neutron energy in Mev. The two distributions compared in fig. 4.3 have been normalized to integrate to the same value. It is seen that there is good agreement between the simulated neutron energy distribution and that measured experimentally.

Equation (4) is used to calculate the angles (ϕ_{LAB}) in the laboratory frame between the neutron directions and the line of flight of their parent fragment. Having determined the angles ϕ_{LAB} and χ (the azimuthal angle) of emission of every neutron emitted in the current fission, the direction cosines specifying the lines of flight of the neutrons in the laboratory frame are calculated. At this stage in the programme the laboratory energies and directions of all the neutrons emitted in the current fission are known and the angular distribution of neutrons relative to the fission axis, as well as the n-n angular correlation may be calculated.

(iii) Calculation of the Neutron Angular Distribution

In order to make the computer simulation as efficient as possible it

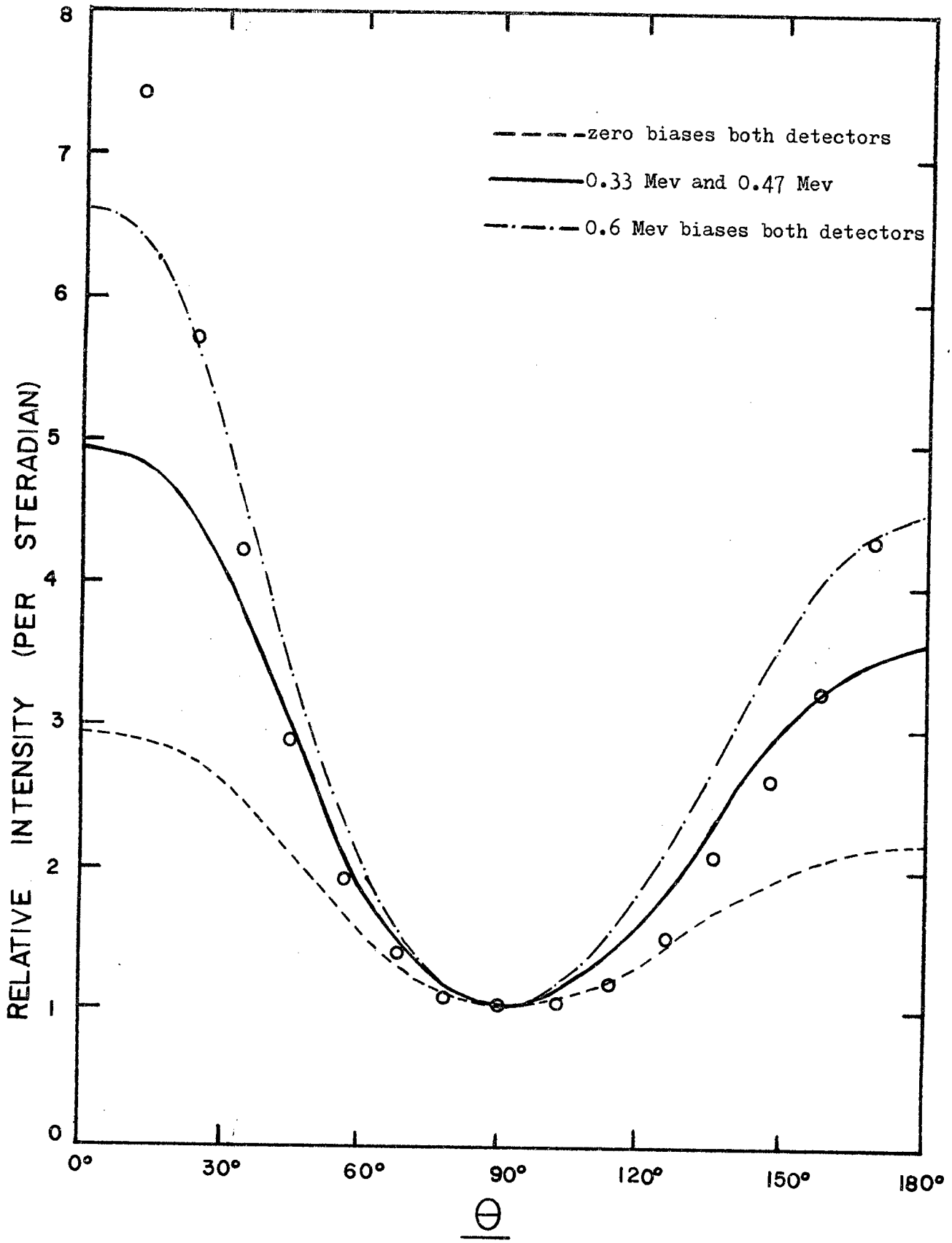

Fig. 4.4: Three simulated neutron angular distributions (lab) relative to the fission axis. The angle θ is measured relative to the light fragment direction.
The data points are those of Bowman et al (Bo 62)
Curves and data points are normalised at $\theta = 90^{\circ}$.

is assumed that every neutron emitted in every fission enters a detector. For each fission neutron a random choice is made as to which detector is entered. The efficiency $\varepsilon(E)$ for detection of the neutron by the detector is calculated from the formula given in section 2.8.

After calculating the detection efficiencies for each neutron, the contribution they make to the angular distribution of neutrons relative to the fission axis is determined as follows. A detected weight equal to $(\varepsilon/\sin\phi_{LAB})$ is calculated for each neutron depending on the angle ϕ_{LAB} between the line of flight of the neutron and the fission axis, and the efficiency ε for detecting the neutron. Then the detected weight of each neutron is added to the element corresponding to ϕ_{LAB} (rounded to the nearest 1°) in the angular distribution array. The accumulated distribution is therefore proportional to the differential cross section or angular distribution which would be measured by a neutron detector placed at different angles ϕ_{LAB} to the fission axis.

Fig. 4.4 shows three simulated neutron angular distributions corresponding to detector bias levels of:

(a) zero biases on both detectors - this gives the "true" angular distribution of neutrons.

(b) 0.33 Mev bias on the "NE 213 detector" and 0.47 Mev on the "Anthracene detector" - this corresponds to the experimental set-up used in run series III.

(c) 0.6 Mev bias levels on both detectors.

The three distributions have been normalized to unity at $\theta = 90^{\circ}$ in this figure. The relative intensities of the un-normalized curves (a), (b) and (c) at $\theta = 90^{\circ}$ are 3.3 : 1.5 : 1. The increased peaking of the distributions at small angles to the fission axis with increasing

bias levels is to be expected intuitively since the higher bias levels discriminate against the low energy neutrons concentrated in the region perpendicular to the fission axis. Also plotted in fig. 4.4 are the experimental data obtained by Bowman et al (Bo 62) from their study of the angular distribution of prompt neutrons from ^{252}Cf spontaneous fission. The differences between the simulated distributions and the observations of Bowman et al are discussed in chapter 5.

(iv) Calculation of the n-n Angular Correlation in the Laboratory Frame

For each fission, all possible combinations of two neutrons are considered in calculating the n-n angular correlation. A detected weight equal to $(\varepsilon_{n_1}\varepsilon_{n_2}/\sin\theta_{n_1 n_2})$ is calculated for each n-n pair depending on the efficiencies for detecting the neutrons n_1 and n_2 and the angle $\theta_{n_1 n_2}$ between their (lab) directions of emission. Then the detected weight of each n-n pair is added to the element corresponding to $\theta_{n_1 n_2}$(rounded to the nearest 1°) in the n-n angular correlation array. The accumulated distribution is therefore proportional to the angular correlation which would be measured in the laboratory by two neutron detectors at relative angle $\theta_{n_1 n_2}$(subtended at the ^{252}Cf source).

Fig. 3.6 shows three simulated n-n angular correlation curves corresponding to the detector bias levels (a), (b) and (c) defined in part (iii) of section 4.2. The three curves have been normalized to unity at 90°. The normalized values of $R(\theta)$ obtained from run series III are also plotted in fig. 3.6. In view of the striking discrepancy between the experimental points and the simulated curves at angles below about 40°, the Monte Carlo programme was modified so as to allow

(a) polar emission of neutrons

and (b) localized emission of neutrons from randomly chosen small regions of the fragment surfaces.

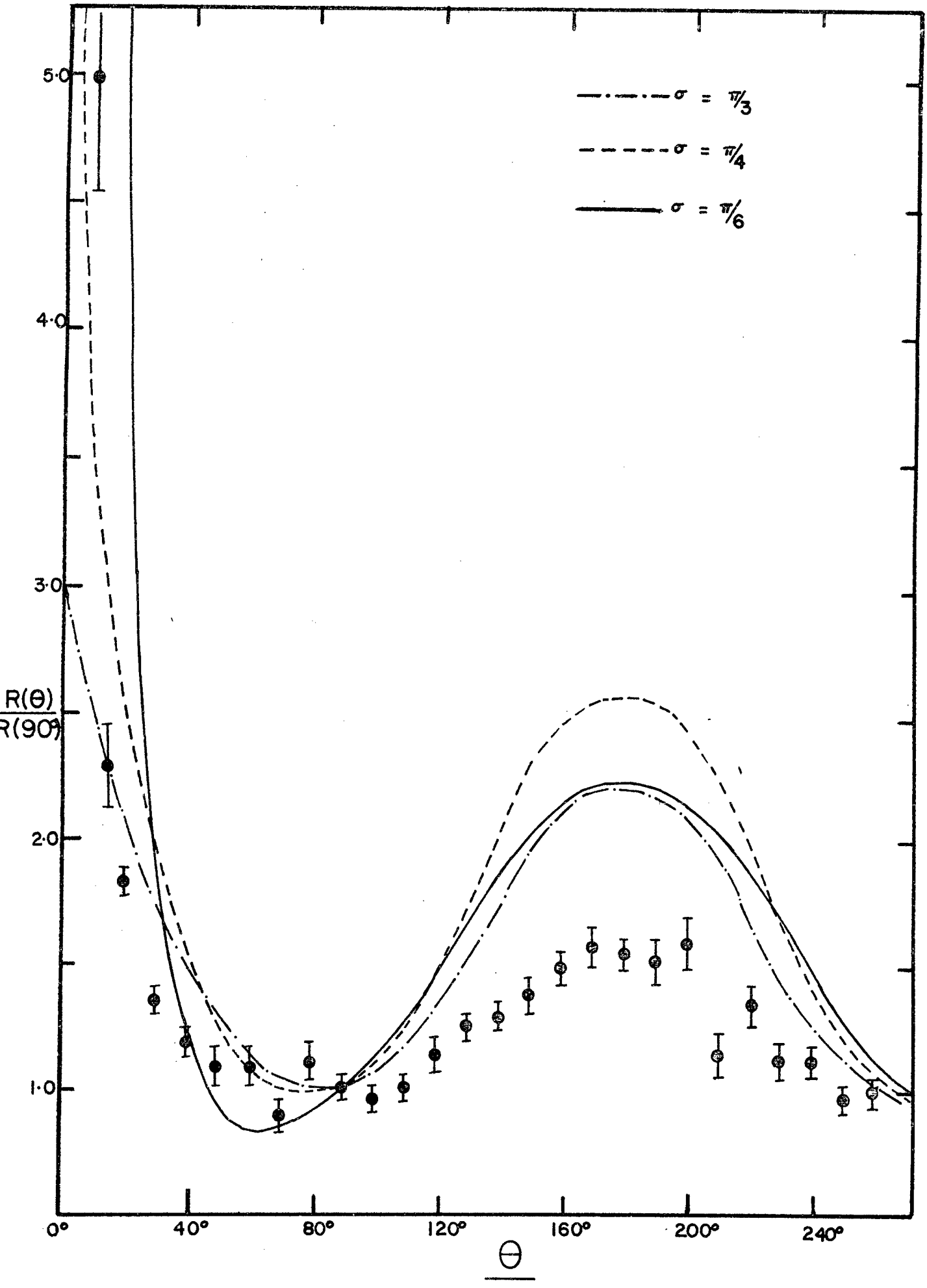

Fig. 4.5: n-n angular correlation
dashed lines are polar emission, solid line localized emission,
data points from run series III. Curves and data normalized at θ = 90°

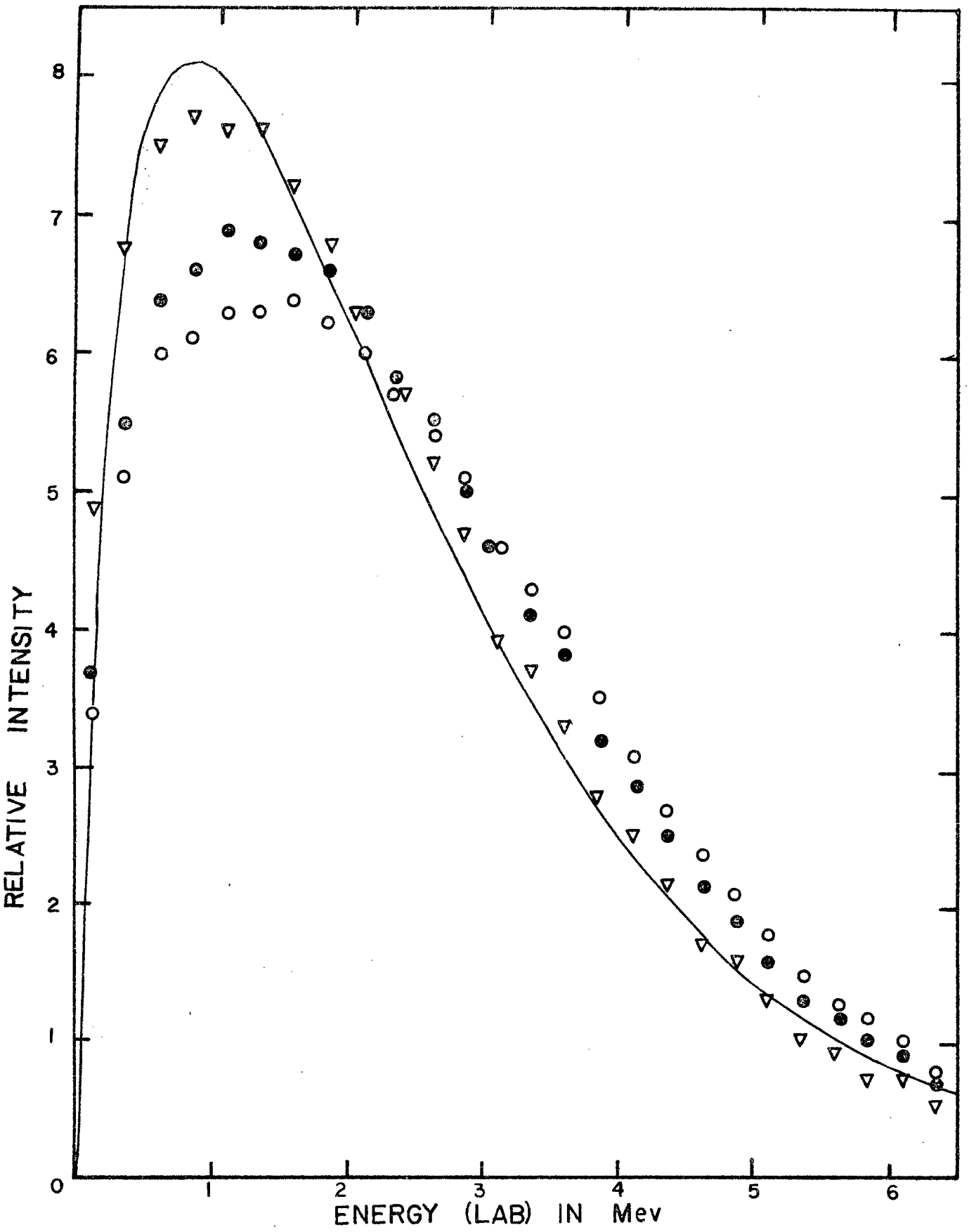

Fig. 4.6: ^{252}Cf Fission Neutron Energy Spectrum
Solid Curve: Watt distribution
Triangles : Localised neutron emission with $\sigma = \pi/6$
Circles : Polar neutron emission with $\sigma = \pi/4$
Solids : " " " " $\sigma = \pi/3$

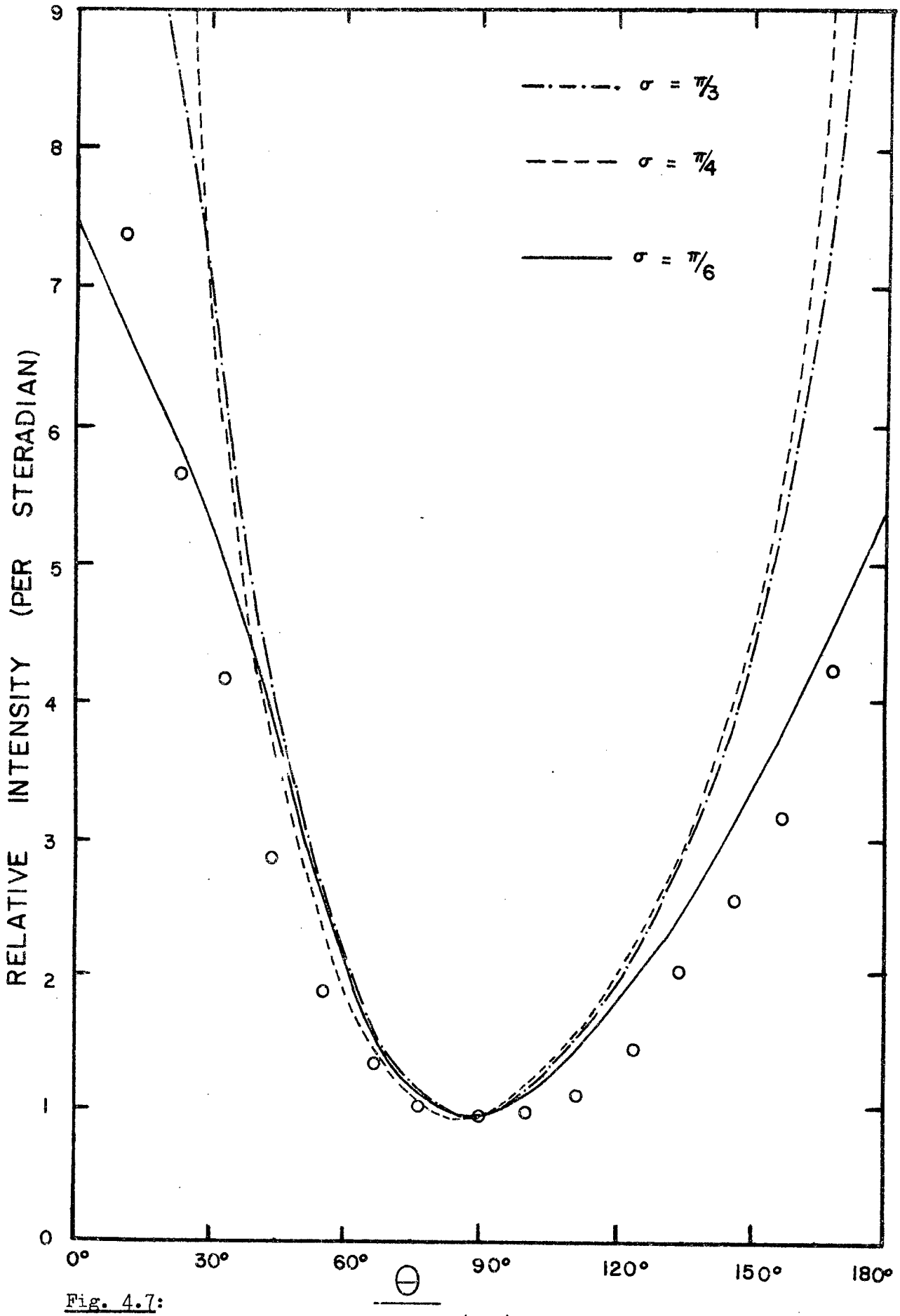

Fig. 4.7:

The angular distribution (lab) of neutrons relative to the fission axis. The angle Θ is measured relative to the light fragment direction. The Data Points are those of Bowman et al (Bo 62)
Dashed Curves: Polar Neutron Emission
Solid Curve : Localized Neutron Emission

(v) Simulation of Polar Neutron Emission

As already outlined in chapter 1, the possibility that collimated polar neutrons may be emitted from the fission fragments arises from the evidence of polar alpha emission in ternary fission (Ha 71). In the absence of any experimental evidence of their nature or existence, the parameters governing polar neutron emission in the simulated fissions were chosen with little physical basis.

In the simulation it is assumed that polar neutrons are only emitted by highly excited fragments. Thus polar neutron emission is restricted to those light fragments having masses $\geqslant$ 110 amu and heavy fragments having masses $\geqslant$ 148 amu. Further, it is arbitrarily assumed that 50% of the neutrons emitted from fragments in these mass ranges are polar. The only difference between simulated fissions involving polar and evaporated neutron emission is in the direction of neutron emission which, for polar neutrons, is chosen from a sharply peaked Gaussian distribution having a mean 0 (corresponding to emission along the fission axis) and standard deviation of either $\pi/4$ or $\pi/3$ radians. The effects on the n-n angular correlation, the fission neutron energy spectrum, and the angular distribution of neutrons relative to the fission axis of the inclusion of a polar neutron component in the emission process are illustrated in figs. 4.5 - 4.7.

(vi) Simulation of Localized Neutron Emission

As in the case of polar neutron emission, there is no experimental evidence for the localized emission of neutrons from the fragments. The parameters governing neutron emission of this type were therefore also chosen arbitrarily.

The method used in the simulation of localized emission is essentially the same as that used to simulate polar neutron emission. The only difference is that in each fission the directions of emission of the neutrons are chosen from Gaussian distributions about randomly orientated emission axes set up in each fragment. This means that while there is no preferred direction of emission of neutrons in the fragment frames when averaged over many fissions, the neutron directions are strongly correlated about the emission axes in individual fissions.

The n-n angular correlation that results if all fission neutrons are emitted through a process of localized emission where the neutrons are confined to a Gaussian distribution of standard deviation $\pi/6$ radians is shown in fig. 4.5. The resulting energy and angular distributions of the neutrons are shown in figs. 4.6 and 4.7.

C H A P T E R F I V E

DISCUSSION

5.1 Checks on the Experimental Data

5.2 Possible Spurious Effects in the Experiment

5.3 Checks on the Simulation

5.4 Conclusions

5.5 Direction of Further Research

Comparison of the experimental measurements of the coincidence ratio $R(\theta)$ and the theoretically calculated n-n angular correlation (see fig. 3.6) show that while there is good agreement for angles larger than about 45° there is a striking disagreement at small angles. Before speculating on the significance of the small-angle peaking it is necessary to examine more closely both the experimental data and the computer simulation to check that the observed peak is in fact a "real" effect.

5.1 Checks on the Experimental Data

(i) Examination of the results of run series III shows that there is a fairly smooth variation in the angular distribution of $R(\theta)$ which is approximately symmetric about $\theta = 180^{\circ}$. Exceptions to this smooth variation are mainly the points at angles greater than 180°. The scatter evident in these points is undoubtedly the result of the fact that only two measurements of $R(\theta)$ were made at each angle θ beyond 180°.

(ii) The effects of variations in the efficiencies (ε) of the detectors, as evidenced by the plot of the singles rates vs. run number (fig. 3.2), are circumvented both by the choice of the ratio $R(\theta)$ which is independent of ε, and also by the averaging effect of making several short runs at each angle.

(iii) The internal consistency of the individual measurements of $R(\theta)$ obtained in each of the run series is convincing evidence of the reliability of the data.

5.2 Possible Spurious Effects in the Experiment

(i) Turning attention to the experimental methods themselves, it would

seem that the most likely cause of the small-angle peaking (if it is not the result of an n-n angular correlation) is the scattering of single neutrons from one detector to the other. However the runs carried out with the Am-Be source show that the contribution of this effect to the value of $R(\theta)$ at small angles is extremely small. The checks carried out with the ^{252}Cf source by measuring $R(\theta)$ for a fixed angular separation θ of the detectors but at different detector-source distances present even stronger evidence that the contribution of single neutron scatterings to the coincidence rate is small.

(ii) Coincidences resulting from the (simultaneous) detection of two or more high energy charged particles from a cosmic ray induced air shower are another possibility to be considered. It seems unlikely that the observed large increase in the coincidence rate at small angles is caused by air shower particles in view of the large area (of the order of hundreds of square metres) covered by the showers and their low incidence rate (about 15 showers per hour at sea level). (Ro 64)

The overall conclusion is that the small-angle peaking of $R(\theta)$ results neither from spurious effect(s) in the experiment nor the analysis of unreliable experimental data.

5.3 Checks on the Simulation

Several checks on the reliability of the results of the computer simulation of neutron emission from ^{252}Cf are possible.

(i) The energy spectrum of the neutrons emitted in the simulated fissions

agrees well with the Watt spectrum used to describe the spectrum observed experimentally. This is shown in fig. 4.3.

(ii) In fig. 4.4 three simulated angular distributions (corresponding to different bias levels of the detectors) of neutrons relative to the fission axis are compared with the experimental points of Bowman et al (Bo 62). The simulated distributions and the experimental data are normalized to unity at $\theta = 90^{\circ}$. The three bias levels used in the simulations were: zero bias on both detectors, 0.33 Mev and 0.47 Mev, and 0.6 Mev on both detectors. It is not unambiguously clear what the detector bias levels were in the Bowman experiment but it is stated in their paper (Bo 62) that neutrons having velocities below 1 cm/ns (i.e. $E_n = 0.52$ Mev) were not considered in their calculations. This would effectively mean that the bias levels were 0.52 Mev and their measurements of the neutron angular distribution should therefore be comparable with the distribution obtained from the simulation where the biases were 0.6 Mev.

It is seen that the simulated (0.6 Mev) distribution reproduces only the broad features of Bowman's experimental findings. If, instead of normalizing the curves to the experimental data at $\theta = 90^{\circ}$, the integrated angular distributions were normalized, the data and the 0.6 Mev curve would agree fairly well except at the angles $\theta \simeq 0^{\circ}$, 90° and 180°. The discrepancy at 90° could be partially removed by adding a small isotropic scission component as suggested by Bowman et al (Bo 62). However the discrepancies at $\theta \simeq 0^{\circ}$ and 180° would remain. It seems therefore that the evaporation model used in the simulation is unable to reproduce the observed neutron angular distribution at small angles to the fission

axis. This lends support to Bowman's finding of an excess of neutrons along the fission axis over that expected from an evaporation model.

(iii) In order to check that the neutrons were being emitted isotropically in the fragment frames, a simulation was carried out in which the fragments were assumed to be at rest in the laboratory frame. As expected, the resulting angular distribution (lab) of neutrons relative to the fission axis was isotropic and the neutron directions in the laboratory frame were uncorrelated.

(iv) As further checks, the total number of neutrons (ν) emitted in every simulated fission, as well as the mass distribution of the fragments, were tallied. Close agreement was found between the simulation and experiment in both respects.

5.4 Conclusions

On the strength of the evidence presented above it is clear that the small-angle peaking in the experimental data of $R(\theta)$ is a "real" effect, and that it represents a significant deviation from the predictions of the evaporation model. It is apparent that this peaking must be caused by some sort of bunched or localized emission of neutrons from the fragments.

A rough calculation based on a comparison of the experimental data and the simulated curves in fig. 3.6 shows that about 30% of the observed n-n angular correlation is not accounted for in terms of the evaporation model. Three possible mechanisms which would give rise to an n-n correlation different from that predicted by the evaporation model have been discussed in chapter 1. Of these three mechanisms, the cascaded emission of neutrons can certainly be

ruled out owing to the fact that the experiment necessarily averaged over all fragment masses and initial states.

The possibility of bunched emission of neutrons from the fission fragments is enhanced by the large number of neutrons emitted in ^{252}Cf spontaneous fission ($\bar{\nu} = 3.74$). In roughly 90% of all fissions two or more neutrons are emitted from one fragment and in about 30% of fissions three or more neutrons are emitted from the same fragment (Hy 64). The final state interaction between two or more neutrons simultaneously emitted from the same fragment could lead to these neutrons being emitted in a low relative momentum state. This would enhance the n-n angular correlation at small angles in the laboratory frame. Even the possibility of a 3n final state interaction might be relevant. Although the dineutron is known to be unbound by about 100 keV (Mc 70), there is recent speculation as to the possible existence of a bound state of the trineutron. Such a state might enhance the n-n angular correlation observed in fission.

A more likely origin of the observed strong n-n angular correlation at small angles is through the emission of an excess of neutrons collimated along the fission axis. Although there is no direct experimental evidence for the existence of these "polar neutrons", the possibility that they may be emitted arises from the finding that about 5% of the alpha particles emitted in ternary fission come from the polar regions of the fission fragment (Ha 71). Several authors have speculated on the possible existence of polar neutrons (e.g., Te 59, De 48, Bo 62).

In chapter 4 the method used to simulate the polar emission of neutrons in ^{252}Cf spontaneous fission is described. The effects of the inclusion of this polar neutron component on the n-n angular correlation are seen in fig. 4.5. From the results it seems likely that by making the correct choice of parameters

an angular correlation closely resembling that observed experimentally could be produced. However, an examination of figs. 4.6 and 4.7 shows that the introduction of a polar neutron component having the same energy spectrum as the evaporated neutrons leads to a fission neutron energy spectrum having a higher mean energy than that observed experimentally, and a neutron angular distribution very much more strongly peaked along the fission axis than the measurements of Bowman et al (Bo 62) suggest. The problem of the differences in the neutron energy spectra could be resolved by assuming that the polar neutrons have a lower mean emission energy than the evaporated neutrons, but there is little physical basis for making this assumption. A side effect of this assumption would be a decrease in the sharp peaking of the neutron angular distribution at small angles to the fission axis as a result of the lower efficiency for detection of the polar neutrons. This would also decrease the n-n correlation at small angles.

It seems therefore that it may be possible to reproduce the observed n-n angular correlation and still be consistent with all other experimental observations on ^{252}Cf spontaneous fission if it is assumed that a certain percentage of the fission neutrons are emitted from the polar regions of the fragments with a lower mean energy than the evaporated neutrons.

A further mechanism proposed in chapter 1 to account for the observed n-n angular correlation is the localized emission of neutrons from the surfaces of the fragments resulting, in a classical picture, from the constructive interference of "tidal waves" of nuclear matter. In this picture, neutrons are emitted at the nodes of a standing wave on the surface of the fragment. The directions of emission of these neutrons need not necessarily be strongly correlated in the fragment frame to give a strong n-n angular correlation in the laboratory frame. An n-n angular correlation in the laboratory will

automatically result through the effects of the fragment motion if the neutrons are emitted from the same region of the surface of the fragment. The method used to simulate neutron emission through this mechanism is described in chapter 4.

In fig. 4.5 (solid curve) it is seen that the tidal wave model, with suitable parameters, could produce an n-n angular correlation closely resembling that observed. Furthermore, both the neutron energy spectrum (fig. 4.6) and the angular distribution of the neutrons relative to the fission axis (fig. 4.7) closely resemble the observed distributions. These points strongly favour the tidal wave model over the polar emission model as a mechanism for the emission of neutrons from the fission fragments. For a fuller understanding of the mechanism, and in order to have some physical basis for the parameters used, it will be necessary to study the motion of waves on the surface of a sphere.

5.5 Direction of Further Research

An interesting feature of the measured distribution of $R(\theta)$ is the fact that its value seems to continue to increase at angles θ smaller than those studied. It would therefore be of interest to measure the values of $R(\theta)$ at even smaller angles θ, preferably by using a more powerful ^{252}Cf source to obtain higher count rates at small angles (where the detector-source distances are large).

In future experiments the background should be investigated more thoroughly. The possible contribution of the cosmic background was not realised until after the present measurements were completed.

The coincidence rate from single neutron scatterings could be estimated more accurately by using an Am-F neutron source instead of an Am-Be source.

This is because the energy spectrum of the neutrons emitted by the Am-F source more closely resembles the ^{252}Cf fission neutron spectrum.

This research programme should also be extended to other nucleides such as ^{235}U to look for evidence of a similar n-n angular correlation to that observed for ^{252}Cf. In the case of ^{235}U this would serve as a follow up to the work of De Benedetti et al (De 48).

In the future, it would be useful to measure the neutron angular distribution relative to the fission axis during the same run series (and using the same detectors) as a set of measurements of the n-n angular correlation. This would mean that the same detector bias levels applied to both distributions thus facilitating the comparison of the results obtained from the simulation and in the experiment.

Finally, it would be particularly useful to do the "complete" experiment, i.e., the measurement of the n-n angular correlation for known values of the angle between the fission axis and one or both detectors. This experiment would provide a simple test of the existence or otherwise of polar neutrons.

A P P E N D I X A

STATISTICAL TREATMENT OF THE DATA

By definition the coincidence ratio $R(\theta) = \frac{\dot{N}_{co}}{\dot{N}_1 \dot{N}_2}$

or $R(\theta) = \frac{(C)(T)}{(N_1)(N_2)}$

where C is the number of coincidences recorded in the run,

N_1 and N_2 are the numbers of singles recorded in each detector,

T is the live time of the run.

Then $\Delta R(\theta) = \sqrt{\left(\frac{\partial R(\theta)}{\partial C}\Delta C\right)^2 + \left(\frac{\partial R(\theta)}{\partial T}\Delta T\right)^2 + \left(\frac{\partial R(\theta)}{\partial N_1}\Delta N_1\right)^2 + \left(\frac{\partial R(\theta)}{\partial N_2}\Delta N_2\right)^2}$

It is found that $\Delta R(\theta) \simeq \frac{\partial R}{\partial C}\Delta C$ (1

It is well known that if N particles are counted in an experimental period, the standard deviation of the result is $\sqrt{N}$ (Br 66). Thus the standard deviation ΔC of C is $\sqrt{C}$. Equation (1) was used to find the standard deviation $\Delta R(\theta)$ of the coincidence ratio $R(\theta)$.

The individual measurements of $R(\theta)$ at each angle θ were combined to give a weighted mean value $\bar{R}(\theta)$. Each measurement of $R(\theta)$ was assigned a weight (W_s) proportional to the reciprocal of the square of its standard deviation $\Delta R(\theta)$. The weighted mean value $\bar{R}(\theta)$ is given by

$$\bar{R}(\theta) = \frac{\sum W_s R_s(\theta)}{\sum W_s} \qquad \text{(To 72)}$$

The standard deviation $\Delta\bar{R}(\theta)$ of the weighted mean was determined using the relation:

$$\frac{1}{\left[\Delta\bar{R}(\theta)\right]^2} = \sum_i \frac{1}{\left[\Delta R_i(\theta)\right]^2}$$

APPENDIX B

LISTING OF THE MONTE CARLO PROGRAMME

----- THIS PROGRAMME SIMULATES ^{252}Cf FISSION NEUTRON EMISSION -----

```
      INTEGER PSI
      DIMENSION MSPEC(47),NLSPEC(10),NHSPEC(10),VL(10),
     1VH(10),NSPEC(20),C(3),ULAB(20),VLAB(20),WLAB(20),
     1F(190),FISPEC(190),EMSPEC(47),ELAB(20),EBIAS(2),
     1SINGLE (2),EFFIC (20),EGSPEC (49)
      COMMON IE,C
      DATA IA,IB,IC,ID,IE,IG,IH,IJ/403,596,531,
     1673,685,754,767,848/
      DATA EBIAS /0.6,0.6/
C     -----EBIAS SPECIFIES OPERATING BIASES OF DETECTORS -----
      IDUM = 0
      DUM = 0.0
C     -----NUMBER SPECIFIES NUMBER OF FISSIONS -----
      NUMBER = 4000
      NTIME=0
C     ----- CHOOSE MASS DIVISION,FRAGMENT VELOCITIES,NUMBER OF NEUTRONS
   15 CALL MASSES(IA,M)
      MSPEC(M)=MSPEC(M)+1
      CALL FVELOC (M,VELL,VELH)
      CALL NUFRAG (M,IB,NUL,NUH)
      NLSPEC(NUL+1)=NLSPEC(NUL+1)+1
      NHSPEC(NUH+1)=NHSPEC(NUH+1)+1
      NU=NUL+NUH
      NSPEC(NU+1)=NSPEC(NU+1)+1
      NTIME = NTIME + 1
      IF(NUL.EQ.0.AND.NUH.EQ.0) GO TO 15
      IF (NUL.GT.0) GO TO 5
      GO TO 10
    5 DO 6 NL = 1,NUL
C     ----- CHOOSE NEUTRON ENERGIES IN FRAGMENT FRAME -----
      CALL NVELOC (M,IC,VN)
    6 VL(NL) = VN
   10 IF (NUH.GT.0) GO TO 11
      GO TO 12
   11 DO 7 NH=1,NUH
      CALL NVELOC (M,ID,VN)
    7 VH(NH)=VN
   12 CONTINUE
C     ----- SET UP RANDOMLY ORIENTATED FISSION AXIS -----
      CALL AXIS

      CALL RANNUM (IH,RRAN)
      IF (RRAN.GT.0.5) GO TO 60
      NDETEC = 1
      GO TO 61
   60 NDETEC = 2
   61 CONTINUE
      IF (NUL.GT.0) GO TO 16
      GO TO 22
   16 MXCITE = 0
      IF (M.GE.36) MXCITE = 1
C     ----- BOIL OFF NEUTRONS ISOTROPICALLY IN FRAGMENT FRAME -----
C      - -- IF MXCITE = 1 THEN POLAR BUNCHING -----
      DO 20 I = 1,NUL
      VNEUT=VL(I)
      CALL DIRCOS (C(1),C(2),C(3),VNEUT,VELL,VNLLAB,IG,IJ,U,V,W,FILAB,
     1MXCITE)
      IF (FILAB.LT.0.001) FILAB = 0.001
      LABFI = IFIX ((57.296*FILAB)+0.5)
      ELAB(I) = 0.522729*(VNLLAB**2)
```

```
      EGY = ELAB (I) * 4.0 + 1.0
      IEGY = EGY
      IF (IEGY.GT.49) IEGY = 49
      EGSPEC (IEGY) = EGSPEC (IEGY) + 1.0
      IF (ELAB(I).LT.EBIAS(NDETEC)) GO TO 17
C     ----- DETERMINE DETECTION PROBABILITY KNOWING LAB ENERGY -----
      CALL DETECT (ELAB(I),NDETEC,EBIAS(NDETEC),EFISH)
      GO TO 18
   17 EFISH = 0.0
   18 EFFIC (I) = EFISH
      FISPEC (LABFI + 1) = FISPEC (LABFI + 1) + (EFISH/SIN (FILAB))
      SINGLE (NDETEC) = SINGLE (NDETEC) + EFISH
      NDETEC = NDETEC + 1
      IF (NDETEC.GT.2)NDETEC = 1
      ULAB(I)=U
      VLAB(I)=V
   20 WLAB(I)=W
   22 C(1)=-C(1)
      C(2)=-C(2)
      C(3)=-C(3)
      IF (NUH.GT.0) GO TO 23
      GO TO 24
   23 MXCITE = 0
      IF (M.LE.17) MXCITE = 1
C     ----- BOIL OFF NEUTRONS ISOTROPICALLY IN FRAGMENT FRAME -----
C     ----- IF MXCITE = 1 THEN POLAR BUNCHING -----
      DO 25 I = 1,NUH
      VNEUT = VH(I)
      CALL DIRCOS (C(1),C(2),C(3),VNEUT,VELH,VHLLAB,IG,IJ,U,V,W,FILAB,
     1MXCITE)
      FILAB = 3.141593 - FILAB
      IF (FILAB.LT.0.001) FILAB = 0.001
      LABFI = IFIX ((57.296*FILAB) + 0.5)
      ELAB(NUL+I) = 0.522729*(VHLLAB**2)
      EGY = ELAB(NUL + I) * 4.0 + 1.0
      IEGY = EGY
      IF(IEGY.GT.49) IEGY = 49
      EGSPEC (IEGY) = EGSPEC (IEGY) + 1.0
      IF (ELAB(NUL + I).LT.EBIAS (NDETEC)) GO TO 64
C     ----- DETERMINE DETECTION PROBABILITY KNOWING LAB ENERGY -----
      CALL DETECT (ELAB (NUL + I),NDETEC,EBIAS (NDETEC),EFISH)
      GO TO 65
   64 EFISH = 0.0
   65 EFFIC (NUL + I) = EFISH
      FISPEC (LABFI + 1) = FISPEC (LABFI + 1) + (EFISH/SIN (FILAB))
      SINGLE (NDETEC) = SINGLE (NDETEC) + EFISH
      NDETEC = NDETEC + 1
      IF (NDETEC.GT.2) NDETEC = 1
      ULAB(NUL+I)=U
      VLAB(NUL+I)=V
   25 WLAB(NUL+I)=W
   24 CONTINUE
C     ----- DETERMINE PROBABILITIES FOR DETECTION OF ALL
C           POSSIBLE NEUTRON PAIRS -----
      IF(NU.GT.1) GO TO 26
      GO TO 27
   26 NDASH = NU - 1
```

```
      DO 28 I = 1,NDASH
      JDASH = I+1
      DO 28 J = JDASH,NU
      ZED = (ULAB(I)*ULAB(J))+(VLAB(I)*VLAB(J))+(WLAB(I)*WLAB(J))
      IF (ZED.LT.0.0) GO TO 37
      CORR = 0.0
      GO TO 38
   37 ZED = -ZED
      CORR = 1.0
   38 IF (ZED.GT.1.0) ZED = 1.0
   41 ANGLE = ACOS (ZED)
      IF (CORR.GT.0.5) ANGLE = 3.141593 - ANGLE
      IF (ANGLE.LT.0.001) ANGLE = 0.001
      PSI = IFIX ((57.296*ANGLE) + 0.5)
      EFICIJ = EFFIC (I) * EFFIC (J)
   28 F(PSI) = F(PSI) + (EFICIJ/SIN(ANGLE))
   27 IF (NTIME.GE.NUMBER) GO TO 30
      GO TO 15
   30 WRITE (5,36)
   36 FORMAT(1H1,4X,'FREQ',3X,'ANGLE',28X,'PROBABILITY DISTRIBUTION OF N
     1-N RELATIVE ANGLE')
      MAXEX = 181
      CALL PLOTTO (F,MAXEX)
      WRITE (5,42) NLSPEC,NHSPEC,NSPEC
   42 FORMAT (//2X,'NUBAR DIST FOR LF',1018,///2X,'NUBAR DIST FOR HF',
     110I8,///2X,'TOTAL NUBAR DIST',2015)
      WRITE (5,43)
   43 FORMAT (1H1,4X,'FREQ',3X,'ANGLE',12X,'PROBABILITY DISTRIBUTION OF
     1ANGLE BETWEEN NEUTRON AND LIGHT FRAGMENT')
      MAXEX = 181
      CALL PLOTTO (FISPEC,MAXEX)
      WRITE (5,52)
   52 FORMAT (1H1,4X,'FREQ',2X,'MASS-80',30X,'MASS DISTRIBUTION FOR LIGH
     1T FRAGMENT')
      MAXEM = 47
      DO 53 I = 1,47
   53 EMSPEC(I) = MSPEC(I)
      CALL PLOTTO (EMSPEC,MAXEM)
      WRITE (5,105) SINGLE (1),SINGLE (2)
  105 FORMAT (1H1,4X,'SINGLES IN ANTHRACENE =',F11.4,///
     14X,'SINGLES IN NE-213 =',F11.4)
      WRITE (5,106)
  106 FORMAT (//////,4X,'FREQ',2X,'0-12MEV',30X,'NEUTRON ENERGY DISTRIBU
     1TION IN LABORATORY IN 0.25MEV INTERVALS')
      MAXEG = 49
      CALL PLOTTO (EGSPEC,MAXEG)
      END
```

```
      SUBROUTINE MASSES (IA,M)
C     ----- THIS SUBROUTINE CHOOSES MASS DIVISION -----
      DIMENSION AFRAG(47),XE(2)
      DATA AFRAG/0.02,0.03,0.04,0.05,0.08,0.09,0.12,0.14,0.18,0.24,
     10.30,0.38,0.51,0.60,0.73,0.88,1.05,1.27,1.53,1.82,2.23,
     12.74,3.27,3.72,4.27,4.97,5.59,5.87,5.91,5.73,5.52,
     15.42,5.22,4.85,4.32,3.93,3.54,3.09,2.59,2.16,1.69,
     11.22,0.85,0.53,0.35,0.26,0.24/
      AYMAX = 6.00
    2 DO 1 J=1,2
      CALL RANNUM (IA,RRAN)
    1 XE(J)= RRAN
      XR = 46.0*XE(1)
      M=IFIX (XR+1.5)
      IF (AYMAX*XE(2).GT.AFRAG(M)) GO TO 2
      RETURN
      END
```

```
      SUBROUTINE BUNCH (IJ,VAR,FI)
C     ----- THIS SUBROUTINE CHOOSES AN ANGLE FROM A SHARPLY PEAKED
C                          GAUSSIAN DISTRIBUTION
      DIMENSION U(2),V(2)
    2 DO 1 J = 1,2
      CALL RANNUM (IJ,RRAN)
    1 U(J) = RRAN
      V(1) = 2.0*U(1) - 1.0
      V(2) = 2.0*U(2) - 1.0
      S = V(1)**2 + V(2)**2
      IF (S.GE.1.0) GO TO 2
      X = V(1)*SQRT((-2.0*ALOG(S))/S)
      FI = VAR * X
      IF (FI.LT.0.0) FI = -FI
      IF (FI.LT.0.017) FI = 0.017
      FI = 3.141593 - FI
      RETURN
      END
```

```
      SUBROUTINE FVELOC (M,VELL,VELH)
C     ----- THIS SUBROUTINE DETERMINES FRAGMENT VELOCITIES -----
      DIMENSION DVEL(13)
      DATA DVEL/1.27,1.26,1.25,1.23,1.20,1.15,1.14,1.17,1.18,1.18,
     11.17,1.17,1.16/
      IF (M.LT.41) GO TO 1
      I=M-40
      VELL=DVEL(I)
      J=54-M
      VELH=DVEL(J)
      RETURN
    1 MASSL=79+M
      MASSH=252-MASSL
      VELL=2.2179-(0.007857*FLOAT(MASSL))
      VELH=2.6278-(0.011111*FLOAT(MASSH))
      RETURN
      END
```

```
      SUBROUTINE AXIS
C     ----- THIS SUBROUTINE SETS UP A RANDOMLY ORIENTATED FISSION AXIS
      DIMENSION C(3),XA(3)
      COMMON IE,C
      DO 1 J = 1,3
      CALL RANNUM (IE,RRAN)
    1 XA(J) = RRAN
      SUMSQ = 0.0
      DO 2 J = 1,3
      C(J) = 2.0*XA(J) -1.0
    2 SUMSQ = SUMSQ + C(J)**2
      FACNM = SQRT (1.0/SUMSQ)
      DO 3 J = 1,3
    3 C(J) = FACNM*C(J)
      RETURN
      END
```

```
      SUBROUTINE DIRCOS (P,Q,R,VN,VF,VL,IG,IJ,U,V,W,FILAB,MXCITE)
C     ----- THIS SUBROUTINE CHOOSES DIRECTION OF EMISSION OF NEUTRONS
C           IN FRAGMENT FRAME AND CONVERTS TO DIRECTION IN LABORATORY
      DIMENSION XE (4)
      PI = 3.141593
    2 DO 1 J = 1,4
      CALL RANNUM (IG,RRAN)
    1 XE(J) = RRAN
      IF ( XE(1).GT.SIN(XE(2)*PI)) GO TO 2
      FI = XE(2)*PI
      IF (MXCITE.LT.1) GO TO 5
C     ----- POLAR BUNCHING IF MXCITE = 1 -----
      IF (XE(4).GT.0.3) GO TO 5
C     ----- POLAR EMISSION IN 30 DEGREE CONE -----
      VAR = 0.2741
      CALL BUNCH (IJ,VAR,FI)
    5 VL=SQRT((VF**2)+(VN**2)-(2.0*VF*VN*COS(FI)))
      Z = ((VL**2)+(VF**2)-(VN**2))/(2.0*VL*VF)
      IF (Z.LT.0.0) GO TO 3
      CORR = 0.0
      GO TO 4
    3 Z = -Z
      CORR = 1.0
    4 IF (Z.GT.1.0) Z = 1.0
      FILAB = ACOS(Z)

      IF (CORR.GT.0.5) FILAB = 3.141593 - FILAB
      XI = PI*(2.0*XE(3)-1.0)
      A=COS(FILAB)
      B=SIN(FILAB)
      C=COS(XI)
      D=SIN(XI)
      IF (ABS(R).GT.0.9999) GO TO 57
      E=SQRT(1.0-R**2)
      U = ((( B*C*R*P)-(B*D*Q))/E) + (A*P)
      V = ((( B*C*R*Q)+(B*D*P))/E) + (A*Q)
      W=-(B*C*E)+A*R
      RETURN
   57 U=B*C
      V=B*D
      W=A*R
      RETURN
      END
```

```
      SUBROUTINE NUFRAG (M,IB,NUL,NUH)
C     ----- THIS SUBROUTINE CHOOSES NUMBER OF NEUTRONS
C                       FROM EACH FRAGMENT -----
      DIMENSION ANUBAR(93),ASIGNU(93),U(2),V(2),X(2)
      DATA ANUBAR/0.30,0.34,0.45,0.51,0.58,0.63,0.68,0.85,0.84,0.95,1.07
     1,1.10,1.14,1.25,1.30,1.32,1.32,1.32,1.32,1.35,1.36,
     11.25,1.35,1.39,1.45,1.54,1.56,1.71,1.88,2.03,2.11,
     12.15,2.31,2.43,2.56,2.59,2.75,2.77,2.95,3.07,3.25,
     13.14,3.03,2.64,2.40,1.95,1.40,1.10,0.79,0.50,0.34,
     10.36,0.56,0.68,0.87,1.08,1.26,1.38,1.45,1.53,1.57,
     11.62,1.68,1.70,1.74,1.84,1.89,2.05,2.10,2.15,2.19,
     12.26,2.41,2.46,2.43,2.51,2.61,2.70,2.79,2.85,2.75,
     12.87,2.98,3.01,2.99,3.14,3.04,3.14,3.10,3.18,3.16,3.20,3.20/
      DATA ASIGNU/0.15,0.15,0.16,0.17,0.18,0.20,0.20,0.21,0.23,0.24,0.27
     1,0.30,0.33,0.42,0.52,0.57,0.66,0.72,0.76,0.80,0.78,
     10.70,0.69,0.68,0.66,0.69,0.70,0.74,0.78,0.75,0.80,
     10.79,0.84,0.83,0.89,0.93,0.96,0.95,0.96,0.93,1.02,
     11.03,1.03,1.03,1.04,1.04,1.05,0.75,0.62,0.48,0.40,
     10.35,0.33,0.34,0.41,0.48,0.56,0.62,0.68,0.71,0.77,
     10.80,0.82,0.82,0.85,0.85,0.88,0.96,0.97,0.96,0.98,
     11.00,1.07,1.06,1.01,1.01,1.02,0.94,0.99,1.01,1.00,
     10.88,0.82,0.76,0.96,0.98,0.95,0.90,0.90,0.90,0.90,0.90,0.90/
      ELNUBA=ANUBAR(M)
      HNUBA=ANUBAR(94-M)
      SIGNUL=ASIGNU(M)
      SIGNUH=ASIGNU(94-M)
    2 DO 1 J=1,2
      CALL RANNUM (IB,RRAN)
    1 U(J)=RRAN

      V(1)=2.0*U(1)-1.0
      V(2) = 2.0*U(2)-1.0
      S=V(1)**2+V(2)**2
      IF (S.GE.1.0) GO TO 2
      DO 3 I=1,2
    3 X(I)=V(I)*SQRT((-2.0*ALOG(S))/S)
      NUL=IFIX(ELNUBA+(SIGNUL*X(1))+0.5)
      NUH=IFIX(HNUBA+(SIGNUH*X(2))+0.5)
      IF (NUL.GT.10.OR.NUH.GT.10) GO TO 2
      RETURN
      END
```

```
      SUBROUTINE DETECT (E,NDETEC,EBIAS,EFISH)
C     ----- THIS SUBROUTINE DETERMINES EFFICIENCY FOR DETECTION
C                           OF CURRENT NEUTRON
      IF (NDETEC.GT.1) GO TO 10
C                 -------ANTHRACENE------
      X = 2.54
      ENH = 0.04222
      GO TO 12
C                 -------NE 213-------
   10 X = 2.99
      ENH = 0.046000
   12 XHYD=9.43/(3.46+0.86*E+0.008*E**2)
     1+3.14/(0.18+1.32*E+0.017*E**2)
      EFISH = ((E - EBIAS)/E)*(1-EXP(-ENH*X*XHYD))
      IF (EFISH.LT.0.0) EFISH = 0.0
      RETURN
      END
```

```
      SUBROUTINE RANNUM (IX,RRAN)
C     ----- THIS SUBROUTINE GENERATES UNIFORM RANDOM NUMBERS ON (0,1) --
      IX=IX*3125
      RRAN=FLOAT(IX)/34359738337.D0
      IF (RRAN.LT.0.0) RRAN=-RRAN
      RETURN
      END



      SUBROUTINE NVELOC (M,IX,V)
C     ----- THIS SUBROUTINE CHOOSES NEUTRON ENERGIES IN FRAGMENT FRAME
      DIMENSION COMEN(47),XE(2)
      DATA COMEN/1.60,1.66,1.70,1.75,1.75,1.74,1.73,1.71,1.69,1.66,1.59,
     11.58,1.56,1.54,1.50,1.47,1.44,1.43,1.42,1.40,1.38,
     11.37,1.32,1.34,1.35,1.36,1.34,1.33,1.34,1.39,1.44,
     11.51,1.55,1.62,1.67,1.71,1.75,1.81,1.85,1.91,1.95,
     12.00,2.04,2.08,2.10,2.11,2.12/
      F(E,T) = (E*EXP(-E/T))/(T*T)
      T= 0.5*COMEN(M)
      AY=1.0
      AX=10.0
    2 DO 1 J = 1,2
      CALL RANNUM (IX,RRAN)
    1 XE(J) = RRAN
      IF (AY*XE(2).GT.F(AX*XE(1),T)) GO TO 2
      E=AX*XE(1)
      V = SQRT(E)/0.723
      RETURN
      END



      SUBROUTINE PLOTTO (Y,MAXEX)
C     ----- THIS SUBROUTINE PLOTS THE DISTRIBUTIONS GENERATED -----
      DIMENSION Y(360),LINE(100)
      YMIN = 0.0
      YMAX = 0.0
      DO 60 I = 1,360
      IF (I.GT.MAXEX) GO TO 62
      IF ( Y(I) .GT.YMAX) MAX = I
      YMAX = Y(MAX)
   60 CONTINUE
   62 CONTINUE
      DO 67 I = 1,100
   67 LINE (I) = 1H
      STEP = 100./ (YMAX-YMIN)
      DO 100 I = 1,360
      IF (I.GT.MAXEX) GO TO 110
      J = (Y(I)-YMIN)*STEP + 1
      J = MINO (MAXO(1,J),100)
      LINE (J) = 1H*
      ICORR = I-1
      WRITE (5,85) Y(I),ICORR,LINE
   85 FORMAT (F10.3,I6,' +',100A1,' +')
      LINE (J) = 1H
  100 CONTINUE
  110 CONTINUE
      RETURN
      END
```

REFERENCES

Am 72 Amersham Technical Bulletin 72/7 (1972)

Ba 71 J P Balagna, G P Ford, D C Hoffman & J D Knight, Phys. Rev. Letters 26 No 3 (1971) 145

Bo 39 N Bohr & J Wheeler, Phys. Rev. 56 (1939) 426

Bo 62 H R Bowman, S G Thompson, J C D Milton & W J Swiatecki, Phys. Rev. 126 (1962) 2120

Bo 63 H R Bowman et al, Phys. Rev 129 (1963) 2133

Br 56 F D Brooks, "Progress in Nuclear Physics" 5 (1956) 252

Br 59 F D Brooks, Nucl. Instr. & Meth. 4 (1959) 151

Br 66 H J J Braddick, "The Physics of Experimental Method" Chapman & Hall, (1966), London

Ca 59 E D Cashwell & C J Everett, "A Practical Manual on the Monte Carlo Method for Random Walk Problems", Pergamon Press, (1959) New York

De 48 S De Benedetti, J E Francis, W M Preston & T W Bonner, Phys. Rev. 74 (1948) 1645

Fr 52 J S Fraser, Phys. Rev. 88 (1952) 536

Fr 63 J S Fraser, J C Milton, H R Bowman & S G Thompson, Can. J. Phys. 41 (1963) 2080

Fu 62 R W Fuller, Phys. Rev. 126 (1962) 684

Gl 65 L E Glendenin, J P Unik & H C Griffin, Proc. of the IAEA Symp. on the Physics and Chemistry of Fission, Vol I, (1965) 377

Ha 39 O Hahn & F Strassmann, Die Naturwissenschaften 27 (1939) 11

Ha 69 G C Hanna, C H Westcott, H D Lemmel, B R Leonard, J S Story & P M Attree, Atomic Energy Review 7 (1969) 3

Ha 71 I Halpern, Ann. Rev. of Nucl. Sci. 21 (1971) 282

Hy 64 E K Hyde, "The Nuclear Properties of the Heavy Elements", Prentice Hall, New Jersey, (1964) Vol 3, 257

Ka 63 S S Kapoor, R Ramanna & P N Rama Rao, Phys. Rev. 131 (1963) 283

Kl 68 Gy Kluge & A Lajtai, Phys. Lett. 27B (1968) 65

Kn 72 H H Knox & T G Miller, Nucl. Instr. & Meth. 101 (1972) 519

Lo 73 E A Lorch, Int. J. App. Rad. Isot. 24 (1973) 585

Mc 70 J S C McKee, Rep. Prog. Phys. 33 (1970) 691

Me 73 G K Mehta, J Poitou, M Ribrag & C Signarbieux, Phys. Rev. C7 (1973) 373

Mi 58 J C D Milton & J S Fraser, Phys. Rev. 111 (1958) 877

Mi 65 J C D Milton & J S Fraser, Proc. of the IAEA Symp. on the Physics and Chemistry of Fission, Vol II, (1965) 39

Mi 68 J H Mize & J G Cox, "Essentials of Simulation", Englewood Cliffs, Prentice Hall (1968)

Na 70 E Nardi & Z Fraenkel, Phys. Rev. C2 (1970) 1156

Na 71 D M Nadkarni, Proc. Conf. on Neutron Induced Fission, I.N.D.C., Bombay (1971) 89

No 62 R A Nobles, Phys. Rev. 126 (1962) 1508

Ow 60 G E Owen & C D Swartz, "Fast Neutron Physics", Part I, ed. J B Marion & J L Fowler (Interscience, New York (1960)) page 211

Ra 71 V S Ramamurthy, Proc. Conf. on Neutron Induced Fission, I.N.D.C., Bombay (1971) 65

Ro 64 B Rossi, "Cosmic Rays", McGraw-Hill (1964)

Sc 65 H W Schmitt, W E Kiker & C W Williams, Phys. Rev. 137 (1965) B837

Sc 66 H W Schmitt, J H Neiler & F J Walter, Phys. Rev. 141 (1966) 1146

Sh 66 Y A Shreider, "The Monte Carlo Method; the Method of Statistical Trials", Pergamon Press (1966) Oxford

Si 72 C Signarbieux, J Poitou, M Ribrag & J Matuszek, Phys. Lett 39B (1972) 503

Sk 63 K Skarsvåg & K Bergheim, Nucl. Phys. 45 (1963) 72

Sl 71 R J Slobodrian, Rep. Prog. Phys. 34 (1971) 175

St 65 W E Stein, Proc. of the IAEA Symp. on the Physics and Chemistry of Fission, Vol I (1965) 502

Te 59 J Terrell, Phys. Rev. 113 (1959) 527

To 72 J Topping, "Errors of Observation and their Treatment", Chapman and Hall, (1972), London

We 37 V F Weisskopf, Phys. Rev. 52 (1937) 295

Wh 59 S L Whetstone, Phys. Rev. 114 (1959) 581

Wh 63 S L Whetstone, Phys. Rev. 131 (1963) 1232

Wi 47 R R Wilson, Phys. Rev. 72 (1947) 189